

SLAC - PUB - 3727

July 1985

(I)

HIGH RESOLUTION DRIFT CHAMBERS*

J. VA'VRA

*Stanford Linear Accelerator Center
Stanford University, Stanford, California, 94305*

ABSTRACT

High precision drift chambers capable of achieving $\leq 50 \mu\text{m}$ resolutions are discussed. In particular, we compare so called cool and hot gases, various charge collection geometries, several timing techniques and we also discuss some systematic problems. We also present what we would consider an "ultimate" design of the vertex chamber.

Extended version of paper presented at the
S. Miniato Meeting on Future High Energy Machines,
Florence, Italy, May 22-25, 1984.

Also submitted to Nuclear Instruments and Methods

* Work supported in part by the Department of Energy, contract DE-AC03-76SF00515 and by CERN.

1. Introduction

High precision drift chambers will play an important part of high energy experiments for the foreseeable future. This is primarily because they can be built large enough to have sufficient redundancy with existing technologies and still be financially accessible. Single track resolution of 20-50 μm for 1 cm of drift and double track resolution of about 100-600 μm seems to be possible. There has been substantial progress in recent years mainly in the following areas:

1. Improvement in understanding low diffusion gases both experimentally and through model calculations.
2. Introduction of new collection optics arrangements.
3. Improvements of the electronics by introduction of:
 - (a) low noise front end hybrid amplifiers and
 - (b) fast (≥ 100 MHz) digitizers.
4. Improvements in understanding the detection process via the introduction of detailed computer simulation programs.
5. Introduction of new technology (Be beam pipes, carbon fibers, high precision machining).

This talk reviews these improvements and tries to present a judgment whether some of these goals are actually achievable and under what conditions. In particular we discuss a choice between so called “cool” and “hot” gases and various charge collection arrangements. We also review the present understanding of a comparison of the leading edge and the center of gravity timing.

Many aspects, however, are not discussed and we refer the reader to a recent review of this subject by G. Charpak and F. Sauli [1].

2. Theoretical Discussion

We present two methods to estimate drift chamber resolution. *The first method* is simple and clearly transparent, however, it does not necessarily provide a sufficient insight into the details of the detection process. With this method we concentrate mainly on a comparison of the “cool” and “hot” gases. *The second method* is Monte Carlo simulation, which is unfortunately much less transparent, nevertheless it is probably the only way to include a sufficient amount of detail about the detection process involving an intricate interplay of many variables. Here one must exercise a careful judgment about what effects are important to include.

2.1 SIMPLE METHOD

In this method one usually separates the individual contributions to the final tracking resolution as follows (neglecting the systematic error contributions for the moment):

$$\sigma^2 = \sigma_{\text{diffusion}}^2 + \sigma_{\text{ionization}}^2 + \sigma_{\text{track}}^2 \quad (1)$$

The track width contribution σ_{track} is generally negligible if we make our analysis insensitive to the presence of energetic electrons by rejecting off-track samples and if we neglect the fact that the resulting residual distributions are not truly gaussian. The $\sigma_{\text{ionization}}$ term is composed of two contributions. The first contribution comes from an occasional presence of very large ionization clusters (Landau effect) and the second one comes from the fluctuations in finite ionization statistics, both contributions coupled with the nonisochronous charge collection of the typical drift cells. The relative size of the first two terms in eq. (1) generally depends on the choice of gas, electronics, method of charge collection and the method of data analysis. As we will see later either term can dominate depending on the particular case.

Let's consider the first term $\sigma_{\text{diffusion}}$ in eq. (1). We assume initially that the diffusion is spherically symmetric. Based on Einstein theory one electron time dispersion of an original point-like charge distribution is $\sigma_x(1 \text{ electron}) = \sqrt{2Dt}$, where t is the drift time and D is the diffusion coefficient. This can be rewritten as $\sigma_x(1 \text{ electron}) = \sqrt{2\epsilon_k X/eE} = \sqrt{(2\epsilon_k X)/(E/p)} \times 1/\sqrt{p}$ where ϵ_k is the electron characteristic energy, E is the electric field, p is the pressure and X is the drift distance. From this we can see two useful and practical dependencies. For a range of operation where $\epsilon_k \sim \text{const}$ and $X \sim \text{const}$, $\sigma_x(1 \text{ electron}) \sim 1/\sqrt{E}$, and for a case where $E/p \sim \text{const}$ we get $\sigma_x(1 \text{ electron}) \sim 1/\sqrt{p}$ since ϵ_k is E/p dependent. Finally, because of the diffusion dependence on the distance, the resolution data are usually fitted with $\sigma^2 = \sigma_0^2 + \delta \cdot x$ function.

Now we introduce a definition of a *cool* gas as a case where $\epsilon_k = kT$, where k is the Boltzman constant and T is the temperature of the gas. If the gas operates within this limit, we call it a thermal limit operation and $\sigma_x(1 \text{ electron}) = \sqrt{2kTX/eE}$. An example of a cool gas is CO_2 . Figure 1 indicates that somewhere around $E \sim 2 \text{ kV/cm}$ and 1 atm of pressure, the drifting electrons begin to be *heated* and $\sigma_x(1 \text{ electron})$ departs from the thermal limit. This illustrates the need to tune the *cool* gases for an optimum operating point. Figure 2 indicates an example of such tuning for three examples of the *cool* gases. One can conclude that at the optimum, one can achieve $\sigma_x(1 \text{ electron}) \sim 50\text{-}80 \mu\text{m}$ at 1 atm of pressure for 1 cm of drift. One should point out that another feature of the *cool* gases is that the drift velocity has a linear dependence on the electric field E and the gas density N , namely

$$V_{\text{drift}} = \frac{1}{2} \frac{e}{m} \left(\frac{E}{N} \right) \frac{1}{(\sigma \bar{v})} ,$$

where m is the electron mass, e is its charge, σ is the momentum transfer cross-section and \bar{v} is the mean electron velocity [2]. The drift velocity of the *cool* gases is slow because of a large value of the momentum transfer cross section, i.e., the gas appears to be *viscous* to the drifting electrons.

By comparison, the typical gases used in drift chambers today begin to be *hot* at rather low values of the electric field gradient, as can be seen in the example of fig. 3. Typically, we can parametrize the increase of the electron characteristic energy as $\epsilon_k \sim (E/p)^\alpha$. The typical single electron diffusion in *hot* gasses can be seen in fig. 4. In such gases one could parametrize the single electron diffusion as

$$\sigma_x(1 \text{ electron}) = \sigma_x^0 \sqrt{\left(\frac{E}{p}\right)^\alpha \frac{X}{E}} \quad \text{for } E > E_c$$

where σ_x^0 is a normalization constant taken at 1 kV/cm, 1 atm and 1 cm drift. Typically, one has $\sigma_x^0 \sim 150\text{-}600 \mu\text{m}$, i.e., a rather large value.

So far we have assumed the diffusion to be spherically symmetric. In many *hot* gases this assumption is not valid, and one finds that the longitudinal diffusion σ_L can be two to four times smaller than the transverse diffusion σ_x . Figure 5 indicates one example, where $\sigma_L(1 \text{ electron}) \sim 250 \mu\text{m} \sim 1/2\sigma_x(1 \text{ electron})$ normalized for 1 atm, 1 cm of drift, 1 kV/cm electric field and using the JADE gas [3]. Recently there has been progress in calculating these two diffusion parameters for typical gases where the momentum transfer cross-sections are known [35]. Figure 6 illustrates one example of such a calculation [4] for 90% Ar + 10% C₄H₁₀, where one reaches $\sigma_L(1 \text{ electron}) \sim 125 \mu\text{m}$ at 1 atm and 1 cm of drift if one chooses the electric field $E \sim 1.5\text{-}2.0 \text{ kV/cm}$, i.e., a factor of four reduction was realized compared to the transverse diffusion. As we will see later, this result slightly underestimates the author's results in the microjet chamber. In addition, there appears to be some disagreement between the measurement (see fig. 5) and the calculation (see figs. 6 and 26), although the explanation could be either in a slight difference in the gases used or because at larger electric fields the experimental cross-sections used in the calculation [4] are less reliable for this particular mixture. In addition, the role of possible gas impurities in any such measurement cannot be underestimated.

Another example of indirect evidence that one can achieve $\sigma_L(1 \text{ electron}) \sim 120 \mu\text{m}$, even in *hot* gases, is a measurement of Farr *et al.*, [5] shown in fig. 7. They

have measured the tracking resolution to be about $60 \mu\text{m}$ at 1 atm and 1 cm of drift in 75% C_3H_8 +25% C_2H_4 gas. If we assume that $\sigma_{\text{diffusion}} \sim 0.5\sigma_L(1 \text{ electron})$ (this point will be explained later) and that their electronics contribution is negligible, we conclude $\sigma_L(1 \text{ electron}) \sim 120 \mu\text{m}$ for this gas.

We conclude that in the present cool gases one can achieve $\sigma_x(1 \text{ electron}) \sim 50\text{-}80 \mu\text{m}$ and in the best hot gases one could obtain $\sigma_L(1 \text{ electron}) \sim 120\text{-}200 \mu\text{m}$ for 1 cm of drift and 1 atm pressure.

The next question is how do we obtain $\sigma_{\text{diffusion}}$ from a knowledge of $\sigma_x(1 \text{ electron})$ or $\sigma_L(1 \text{ electron})$. This generally depends on the method of detection of the signal.

Leading Edge Timing

The leading edge timing generally samples only a small fraction of the full track sample length because of the nature of charge collection geometry in typical drift chambers (see next chapter). This means that not all of the total N charge clusters arriving at the anode will actually be taken into account. Some of the clusters arrive so late that they cannot contribute to the leading edge timing. In addition, we can assume that $\eta \cdot N \cdot p \cdot n$ is the fraction of the number of electrons having a chance to contribute to the leading edge timing, where η is a measure of efficiency of the charge collection for this particular timing method and can be estimated from the Monte Carlo program [7] by plotting a histogram similar to fig. 10 and determining an effective sample size, p is the pressure and n is an average number of electrons per cluster. In general, η can be influenced by many variables as for instance by the total gain on the anode (later arriving charge can be suppressed by saturation effects), the particular choice of the charge collecting geometry, the choice of gas, and a choice of the operating point. From purely statistical consideration [6] for the first electron timing we would get (if we keep E/p constant as we change the pressure p and $\eta \cdot N \cdot p \cdot n$ is large):

$$\sigma_{\text{diffusion}} \sim \frac{0.91}{\sqrt{\ln(\eta N p n)}} \frac{\sigma_L(1 \text{ electron})}{\sqrt{p}} \quad (2)$$

For typical examples, we get $F = 0.91/\sqrt{\ln(\eta Npn)} \sim 0.5$ (see table 5). The logarithmic dependence in eq. (2) reduces the sensitivity to errors in the estimate of the number of clusters contributing to the timing. One can see that the fastest way to improve the resolution is to increase the pressure. To improve the resolution through an improvement of the collection optics (η) is a much slower way to gain. From table 5 one can conclude that the leading edge timing data can be explained using eq. (2), certainly at the level of difference of about 10-20 μm . To understand the data below this level will require a careful understanding of systematic errors.

This means that for the *cool* gases one can achieve $\sigma_{\text{diffusion}} \sim 10\text{-}20 \mu\text{m}$ at 4 atm and 1 cm of drift. In contrast, in the best *hot* gases one could achieve $\sigma_{\text{diffusion}} \sim 30\text{-}50 \mu\text{m}$ under the same conditions, i.e., to match the result of the *cool* gases we have to go to higher pressure.

Center of Gravity Timing

Let's assume that our electronics (say 100 MHz FADC digitizer) can measure an average time centroid of the arriving charge. From purely statistical consideration we would expect (if we keep E/p constant as we change pressure p and if we assume that the electron cloud is approximately Gaussian in a given timing acceptance window):

$$\sigma_{\text{diffusion}} = \frac{1}{\sqrt{(\eta Npn)}} \cdot \frac{\sigma_L(1 \text{ electron})}{\sqrt{p}}, \quad (3)$$

where N is the total number of charge clusters arriving at the anode (at 1 atm), p is the pressure, η is the fraction contributing to particular timing acceptance window, and n is the number of electrons per cluster. The η can be influenced by a similar set of variables as for the leading edge timing, but in addition we can have variables like a choice of the waveform digitizing electronics (speed of the FADC's) or a method of analyzing the data (a particular choice of weighting scheme of the FADC bins).

Comparing eqs. (2) and (3), one would expect a considerable improvement in the center-of-gravity timing compared to the leading edge timing. Indeed, great improvements in timing resolution were expected by the introduction of the FADC's on the market recently. One can say that the $\sigma_{\text{diffusion}}$ term in eq. (1) has been indeed reduced; however, this has been achieved at the expense of increasing the $\sigma_{\text{ionization}}$ term. This can be fully understood only after we explain the details of the charge collection geometries and we will return to this point later. Here we would only say that, due to the nonisochrony of the charge collection, the fluctuation in ionization statistics will affect the variance significantly and this will cause the predictions using eq. (3) to be always too optimistic.

2.2 MONTE CARLO METHOD

The danger of all Monte Carlo techniques is that they sooner or later become a black box and one loses the feeling of transparency due to an interplay of too many variables. It is not our intention to review all previous attempts to write such codes. We will just describe our contribution to this problem. Before attempting to write such a program, it is very important to select the variables that contribute significantly to the resolution, as well as to keep in mind the final result (apart from pretty pictures). We have attempted to write such a code [7] with the hope of being able to predict the resolution for a previously unknown geometry [8] as well as to find some trick in a possible timing technique [9]. The method consists of including three basic elements of the detection process:

Generate the drift time distribution $i_{\text{drift}}(t)$ by:

- (a) creating the primary ionization in clusters (Landau effect) according to Piuz and Lapique [10],
- (b) drifting each electron within each cluster independently in a two-dimensional electrostatic field,
- (c) using the correct drift velocity in each step,
- (d) including the effect of the magnetic field,

(e) and including the effect of the diffusion (σ_L and σ_x).

Generate the response of the avalanche $i_{\text{avalanche}}(t)$ by:

- (a) including the effect of the motion of the positive ions,
- (b) and including the effect of the avalanche fluctuations.

Generate the response of the electronics $i_{\text{electronics}}(t)$ by:

- (a) using the measured response of the amplifier,
- (b) including the effect of zero-pole filters to perform proper shaping of the final pulse,
- (c) as well as including the effect of cables and noise.

The final drift pulse is then a convolution of the three terms $i(t) = i_{\text{drift}}(t) \times i_{\text{avalanche}}(t) \times i_{\text{electronics}}(t)$. It is important to point out that the method assumes a full linearity in the process of the waveform formation, i.e., all drifting electrons have equal weight. This can be satisfied only at low gains. An example of such pulses can be seen in fig. 8. Once we have created such pulses we can investigate various timing strategies, for instance (a) first electron timing, (b) multiple threshold timing, (c) various strategies with waveform digitizers, etc. As I said, this makes sense only before we build the chamber; once we have data, of course, it is better to use it instead. An example of what appears to be a correct prediction by this program is the conclusion that the 100 MHz digitizer is not fast enough to improve on the simple first electron leading edge timing in the first few centimeters of drift and in a cell structure like a jet chamber using a *fast* gas [9]. We will use several other examples of output from our program during the following text.

Recently there have been other attempts to study the drift chamber using the Monte Carlo techniques [11,12]. For instance, experiment NA34 in CERN [12] used such a program to study the proper shaping of their electronics to obtain an optimum double track separation. None of the previous Monte Carlo programs treated the avalanche entirely correctly. Recently there has been an attempt

in a correct direction, namely the avalanche is treated three-dimensionally [43]. However, the success of such simulations will depend on a knowledge of input data for a particular gas operating at very large electric gradients. Such simulations might be necessary to understand systematics of the detection for resolutions below 10-15 μm .

3. Examples of Charge Collection Geometries

Figure 9 shows typical examples of the charge collecting geometries used in existing prototypes or physics experiments. Table 1 provides typical results. One must admit that most of the results come from the tests rather than the real experiments; however, at the same time one should point out that the serious attempts to reach good resolutions in the vertex chambers are relatively recent.

None of the charge collecting geometries are truly isochronous as in fig. 10(a), although there are variations in the degree of the *isochronity* between various detectors. In an ideal isochronous case all electrons from the track sample would reach the anode at the same time and as a result the η factor in eqs. (2) and (3) would be largest, we would obtain the best multiple hit capability and the center-of-gravity timing would be less sensitive to the finite ionization statistics and the Landau effect. Instead, a more typical charge collection is described in fig. 10(b). However, even in an ideal isochronous case there is one problem. As we significantly incline the track with respect to the anode plane we obtain very nonisochronous charge collection, subject to the same problems as in the case of fig. 10(b). There is only one solution to this problem and that is to decrease the sample size up to the point that we still obtain good single track resolution. In the following examples we will see that one can limit the sample size either (a) physically [11], (b) electrically [13,14], (c) or using software [15]. We will now describe typical examples of the charge collecting geometries as used in existing prototypes.

3.1 JET GEOMETRY

This concept was pioneered by JADE [16] and it is presently considered by many groups for a possible vertex detector. This is primarily because of the simple time-to-distance response, the reasonable multiple hit capability, the low sensitivity of the resolution to the angle of the tracks as well as “clean” electrostatics of the cell. On the negative side of this concept, this cell represents a decreased flexibility in the choice of an operating point, i.e. selection of the gain, electric field and the gas (they have to be “married” together). Also, in view of our previous discussion, the charge collection in the cell is far from isochronous, see fig. 11. Figure 11(a) shows how the clustering (Landau) and the ionization fluctuation affects the randomness in the pulse shapes, a point which will be discussed quantitatively later. The fig. 11(b) shows the effect of the drift distance on the isochronous response, i.e. for tracks going through the anode plane one simply runs out of statistics in the first arriving charge and this effect is responsible for a worsening of the resolution for distances less than wire spacing (the only remedy for this problem is to increase the pressure – see fig. 7). Figure 11(c) shows the charge collection for inclined tracks. Because the bottom of the U-shapes remain relatively unchanged, the resolution as obtained for instance by a leading edge method should remain unchanged, although the multiple hit capability will clearly be worse at larger angles.

One could ask a question whether we can improve somehow the isochrony of this chamber. Figure 12 indicates that one can do it by a suitable choice of the gas behavior [17]. If we operate “behind” the peak in the drift velocity, the electrons drifting near the potential wires (where the field is lower) can pick-up speed and the U-shape response in fig. 11 gets flatter. This is then manifested in shorter drift time distributions and the η -factor in the eqs. (2) and (3) should increase. One can see however that at larger magnetic fields ($B > 5$ kG) this particular method of focusing will stop working. Clearly, the 90% Ar + 10% CH₄ is not the best gas from the plateau behavior and the diffusion point of view and

one would have to try to find a better mixture. One example of a gas with this behavior is 93% Ar + 3% CO₂ + 4% CH₄ [44].

One example of a high resolution application of the jet chamber concept [18] can be seen in fig. 13. The test achieved $\sim 23 \mu\text{m}$ resolution for 4 mm average drift distance using a "hot" gas (75% C₃H₈ + 25% C₂H₄) at 4 atm and using the leading edge electronics. Using the eq. (2) we would expect $\sigma_{\text{diffusion}} \sim 18 \mu\text{m}$ (see table 5), assuming that only 0.8 mm of track sample contributes [7] and that we have ~ 34 clusters in 1 cm of track and ~ 3 electrons per cluster in this gas. The chamber had 2.5 mm wire spacing with the potential wires fully collecting charge and with a simple "switchyard" multiple hit electronics they obtained ~ 1 mm double track separation. One bad feature of this particular arrangement is a ripple in the electrostatic field around the boundaries of the cell. This chamber can be regarded as a predecessor of similar but somewhat larger chambers built for the NA27 experiment at CERN, which is using them for the physics running presently.

A second example is the micro-jet chamber concept [19] seen in fig. 14. The idea here is to further decrease the anode wire spacing (1 mm) to improve the double track separation. In this case it was necessary to use a continuous cathode to limit the field emission problems (if the wires for the cathode were used instead). The continuous cathode should increase the chamber lifetime as well as to improve the uniformity of the electrostatic field near boundaries. Finally, we use very thin anode wires (7.8 μm diameter) which can easily drive the amplifier [20] into a slewing rate limited mode reducing the slewing corrections to a minimum. The use of thin wire limits the overall length of the chamber to ~ 10 -15 cm. We would like to mention that these wires proved to be much more resistant against the breakage than one would initially expect. The chamber obtained $\sim 22 \mu\text{m}$ resolution for 2 mm average drift distance in a "hot" gas (90% Ar + 10% C₄H₁₀) at 6.1 atm with a simple leading edge timing. As one can see from fig. 6, its electric field of 1.5-2.0 kV/cm atm was about an optimum from the longitudinal diffusion point of view. We cannot use the eq. (2) in this

particular case because we have not kept E/p constant as we changed the pressure p . We use instead $\sigma_{\text{diffusion}} \sim 0.91/\sqrt{\ln(0.6 \times 6.1 \times 3.0)} \times 130 \mu\text{m}/\sqrt{\text{cm}} \times \sqrt{((14.6 \text{ kV/cm})/6.1 \text{ atm})^{1.3} \times 0.2 \text{ cm}/(14.6 \text{ kV/cm})} \sim 16 \mu\text{m}$, assuming that only ~ 0.2 mm of track sample contributes to the leading edge timing [9] and that we have ~ 30 clusters in 1 cm of track and ~ 3 electrons per cluster in this gas, and the longitudinal diffusion normalized for 1 kV/cm, 1 atm and 1 cm drift is $130 \mu\text{m}/\sqrt{\text{cm}}$. Measuring the average shapes of the drift pulses in the e^+ beam one would conclude that the double track separation is about $600 \mu\text{m}$ using a simple switchyard electronics, and that this could be improved further using ≥ 200 MHz digitizer [21]. The electronics resolution obtained in the test was about only 61 psec and a N_2 laser was used to tune some of the operating points [22]. At higher rates applications one would have to reduce the gain and this would require taking care of slewing either electronically using the constant fraction discriminator [23] or in the software if double threshold electronics would be used [9]. Reference [51] shows an example of low noise high gain electronics with a very tight pulse shaping, which would be suitable for this particular drift chamber concept.

A third example of this structure is the SLD #1 prototype which has been tested at SLAC [24]. With a cool gas of 92% CO_2 + 8% C_4H_{10} at 1 atm the chamber obtained interesting results as seen in fig. 15. The chamber used the leading edge electronics. Using our simple eq. (2) and assuming that ~ 1 mm of the track sample contributes one expects in 1 cm drift $\sigma_{\text{diffusion}} \sim 49 \mu\text{m}$ (see table 5).

Finally, we want to mention a development of the UA1 vertex detector. The 80 cm long jet chamber with 1.58 mm wire spacing achieved ~ 40 - $50 \mu\text{m}$ resolution for ~ 0.5 cm drift in 50% Ar + 50% C_2H_6 gas at 3 atm [45]. Again, we get a good agreement with the eq. (2), if we use 0.6 mm as an effective sample size (see table 5).

3.2 CYLINDRICAL GEOMETRY

Examples of such geometry are the vertex detectors for the Mark II at SLAC [25], the ARGUS at DORIS [26] and the Aachen University test [46]. The former is already producing physics, the second is about to start. The advantage of this concept is that it is a simple geometry requiring a relatively small number of wires. On the negative side, the cell has considerable edge effects – see fig. 16. It is very nonisochronous and has a nonuniform electric field throughout the cell. Nevertheless, the beam test with the ARGUS vertex detector indicates resolutions in the range of 40-80 μm using gases at 1.5-2.0 atm. The Aachen University test achieved $\sim 30 \mu\text{m}$ resolution for $\sim 5 \text{ mm}$ drift distance using 80% CO_2 + 20% C_4H_{10} gas at 1 atm [46]. The results can be seen in fig. 32 and we will discuss them more in chapter 5. One should also mention a modularized concept of hexagonal miniature drift cell proposed recently by Charpak and Sauli [52]. We would also like to mention the vertex chamber prototype utilizing closely packed 7 mm diameter aluminized-mylar tubes which was recently tested by the MAC experiment at SLAC [41]. With the hot standard gases operating at 4 atm they have achieved resolution in the range of 30 μm . The obvious advantage of this system is its simplicity. In addition, the use of continuous cathode improves the chamber lifetime in a high radiation environment.

3.3 SAMPLE RESTRICTING GEOMETRY

Figure 17 shows an example of a geometry where the accepted track sample is restricted physically [11]. As we discussed earlier this should improve the double track separation as well as reduce the sensitivity of the resolution and double track separation to angles of the track with respect to the anode plane. We can see that by using a cool gas at 4 atm, the test achieved a resolution of about 30 μm for 1 cm of drift. Using the eq. (2) and assuming 29 electrons in 0.8 mm of accepted sample at 4 atm we would expect $\sigma_{\text{diffusion}} \sim 17 \mu\text{m}$ (see table 5) for the first electron leading edge timing. As one can see from fig. 17(d) a double

track resolution of about 100-300 μm was achieved. The authors have shown that a further increase in pressure did not achieve a further improvement in the resolution, presumably due to the attachment problems in CO_2 mixtures. Figure 17(e) indicates their proposal of how to implement one version of a restrictive geometry in practice.

3.4 SPECIAL FOCUSING GEOMETRY

We have two examples where an attempt is made to focus the flow of drifting electrons to improve the isochrony of the charge collection. The first example can be seen in fig. 18(a) [13]. This geometry was chosen for a prototype test by the NA34 experiment in CERN. The idea is to use the channeling wires (c) to control the accepted track sample size from ~ 3.5 mm to ~ 7 mm. In this way they could study the sensitivity of the single track resolution as well as the double track separation to the sample size length without the necessary of building different prototypes. In addition the structure separates left-right collection. Figure 18(b) indicates the lines of equal arrival times to the anode for voltages corresponding to the smallest (~ 3.5 mm long) accepted sample length. One can see that the structure is not completely isochronous, in fact only ~ 1.5 mm of the track length contributes to the first charge arrival. Figure 18(d) shows the single track resolution in the "cool" gas of 90% CO_2 + 10% C_4H_{10} at 1 atm. Again, if we use the eq. (2) and assume ~ 1.5 mm of the track sample contributing to the definition of the first electron timing we get $\sigma_{\text{diffusion}} \sim 42 \mu\text{m}$ (see table 5) for 1 cm of drift, i.e. rather close to the measured results. They observed that by varying the track sample length one does not vary the single track resolution (i.e. the first electron timing is derived from the first ~ 1.5 mm of the track length), but one can affect the double track separation (the overall drift time distribution length gets larger for larger accepted track sample). They studied the double track separation using the N_2 -laser and they found $\sim 80\%$ efficiency to find the second track if it is $\sim 600 \mu\text{m}$ apart from the first track. One should also mention that they have developed a drift program [12] to carefully tune shaping

constants of the electronics for a particular mixture with the CO_2 gas. Finally, this collaboration has built the charge restricting structure [38] similar in concept to that indicated in fig. 17(e), but with a 2 mm restricting gap. The single track resolution results are shown in fig. 18(c) and are essentially in agreement with the results of the focusing geometry of fig. 18(a), although, one would expect that the restricting geometry should improve the double track separation.

The second example in fig. 19 comes from the SLD proposal at SLAC and it was studied both experimentally [50] and theoretically using the Monte Carlo program [8]. The collecting geometry resembles the jet focusing geometry, however the potential wires are dropped. One would expect that this structure will enhance somewhat the η factor in the eq. (2) due to an increase in the effective sample size compared to a simple jet geometry. Indeed, comparing fig. 19(b) and fig. 15, we can see a small improvement of the resolution in case of the focusing geometry. Table 5 compares the experimental results with the eq. (2). Solid curve of fig. 19(b) shows more sophisticated Monte Carlo prediction [8]. The real advantage of the focusing geometry over a simple jet geometry is in an improvement of the multiple hit capability.

Figure 35(d) shows one of the prototypes of the Mark II group [47]. The 30 cm long test chamber operating with 92% CO_2 + 8% C_4H_{10} gas at 3 atm achieved $\sim 35 \mu\text{m}$ resolution for 1 cm drift.

3.5 TIME EXPANSION GEOMETRY (TEC)

This concept was originally proposed by Walenta [27] and it is being presently pursued by the LEP3 collaboration [14]. Figure 20 shows the present arrangement during the test. The original concept of pick-up wires to determine the angles of the tracks has been abandoned. A pair of focusing wires are used which by proper biasing control the size of the accepted sample size (typically ~ 2 mm of track length). No attempt to measure individual clusters is made presently, one determines the centroid of the average charge by the 100 MHz FADC electronics. The tail due to the positive ion response is eliminated by a proper shaping

electronics [20] to improve the multiple track capability. The TEC concept when implemented with the mesh electrodes (test used a 250 μm mesh) represents the most ideal geometry because the gain and the drift regions are separated and one has a total freedom to choose the chambers parameters. However, the mesh solution is difficult to implement in practice for larger chambers and the LEP3 group has decided to test a wire grid instead (1.2 mm wire spacing). The present test resolution results with a mesh solution and the “cool” gas 80% CO_2 + 20% C_4H_{10} can be seen in fig. 29. We will discuss them in detail in the last chapter. The measured 3σ double track separation is about $\leq 300 \mu\text{m}$ for small angle tracks ($\sim 0.8^\circ$) at 2 atm.

We should mention that the mesh solution of this concept was tried also at SLAC by F. Villa [28]. The significance of this test is the first use of low diffusion dimethyl ether gas. This test has been recently repeated [48] and fig. 30 indicates the results obtained with the leading edge timing.

3.6 RADIAL DRIFT CHAMBER GEOMETRY (RDC)

Recently a novel method of vertex reconstruction has been proposed by D. Nygren and J. Huth [49]. The detector is based on a slow radial drift in dimethyl ether gas. Figure 31 shows a basic geometry of the charge collection. The reconstruction of tracks is based on the concept that every point in the sensitive volume is mapped by the electric field to a corresponding position on the surface of the anode wire. This position on the anode wire can be defined by an angular coordinate α . To measure α , the authors adopted a concept of pickup wires originally proposed by Walenta [27]. The absence of argon, traditionally a major component in the drift chamber gas mixture, eliminates a strong source of UV photons which can broaden the avalanche growth. Therefore, the dimethyl ether improves the resolution in α -angular coordinate. One should point out that the radial drift ($\theta \sim 90^\circ$) allows to measure $\alpha(t)$ on all drifting ionization with a better accuracy compared to the originally proposed concept where $\theta \sim 0^\circ$ [27]. The most significant feature of this concept is a utilization of all created

ionization for the final timing information. The predicted resolution should follow eq. (3) with $\eta = 1$, i.e. the technique should improve the resolution with a (pressure)⁻¹ dependence. Another advantage of this concept is an absence of the grid structure which is a mechanical complication. On negative side, the expected multiple hit capability is worse compared to what one can achieve in the TEC chamber (see chapter 6) and is basically given by a periodicity of wire structure, i.e. of the order of millimeters.

4. Systematic Effects

It would be unfair not to discuss the most significant systematic effects which will influence the overall resolution obtained over many months of the running needed in a typical physics run. In the previous chapters we have seen very impressive results obtained with the “cool” gases. The question is now if the advantages of the “cool” gas over the “hot” gas in terms of the diffusion and the lower demand on the speed of electronics will not be offset by the disadvantage due to larger sensitivity to systematic effects mainly because the “cool” gases do not operate on the plateau of the drift velocity curve.

There are basically three types of systematic effects. The first one is hopefully constant in time, examples are nonuniform electrostatic field around the cell boundaries, errors in electrostatic deflection, errors in mechanics, fill to fill variations in a gas composition, etc. These errors could be calibrated to some extent for instance by the laser. The second type of systematic error is changing in time in a not necessarily controlled way, examples are nonuniform temperature throughout the volume of the chamber, etc. The third type of systematic error has to do with details of the signal creation and propagation on the wires and the way the electronics handles the pulses.

Table 2 summarizes the sensitivity of the spatial error to an error of 1/1000 in the drift velocity, time, electric field and density for two examples, one using a “cool” gas (TEC chamber) and the second using a “hot” gas and operating on

a plateau (JET chamber). We see that errors in time and velocity affect both concepts approximately equally, however the benefit of operating on the plateau of the drift velocity is seen in the sensitivity to errors in the electric field E and the gas density N . This is because in the “cool” gas concept we have $\Delta v/v = \Delta E/E$ and $\Delta v/v = \Delta N/N$, and in the “hot” gas case we get $\Delta v/v \sim 0.5(\Delta E/E)^2$ [29] – see fig. 21 and $\Delta v/v \simeq O(N)$ (sensitivity goes through the E/p dependence of the drift velocity v). We conclude that the “plateau” operation will protect us much better against drifts in voltage, nonuniformities in the electric field, space charge effects as well as the temperature drifts [30]. The temperature sensitivity can be seen in fig. 22. On the other hand the slow gases will lower a demand on the electronics performance (1/1000 error in time requires the electronics resolution of about 2 ns in the “cool” gas and about 200 psec in the case of the “hot” gas).

We would like to be more specific about the space charge effects. Let’s assume we have a small JET and TEC chambers with 1 cm drift and 1 m long wires. In present e^+e^- storage rings the typical current at high luminosities can be as high as 200 nanoamperes per wire. We would like to ask a question what will be the change in the drift electric field E in the presence of positive ions leaking into the drift volume from the avalanches on the anodes. A simple minded integration of the Poisson equation reveals that the change of the electric field compared to an original setting will follow an equation $\Delta E = \rho^+(X - d/2)/\epsilon_0$, where ρ^+ is a density of the positive ions, X is a position in the anode-cathode gap and d is the length of the anode-cathode gap (1 cm). The maximum change is then $|\Delta E| \leq \rho^+d/2\epsilon_0$. The density of positive ions $\rho^+ = \epsilon NT^+e/V$, where ϵ is the fraction of positive ions leaking into the drift volume, N is the production rate of positive ions (200 nanoamperes), T^+ is total positive ion drift time and V is volume (wire length \times sample size \times d). Table 3 summaries results from three examples. One can see that to lower the drift velocity through lowering the electric field is dangerous because we lower the removal rate of the positive ions. Also, if ϵ would be significantly increased (say $\epsilon \sim 0.5$) the time expansion concept would become sensitive to the space charge effects. In this context we

would like to point out that the physical restriction of the sample size should help to reduce ϵ . As we see in table 3 the plateau operation of the “hot” gases protects us very well against the space charge effects (due to the dependence $\Delta v/v \sim 0.5(\Delta E/E)^2$).

As far as the third systematic error is concerned, we would like to point out that the additional demand on a multiple use of such device would probably worsen its resolution. Long wires, improper termination or stereo layers will bring additional corrections to deal with. Resistive wires in the case of charge division will increase the time slewing corrections. Also the uncompensated cross-talk in combination with the staggering will affect the rise time. However, these problems are too specific to particular examples and we will not discuss them further.

5. Leading Edge Versus Center of Gravity Timing

First of all, let’s assume that we are dealing with high precision drift chambers with maximum drift length of about 2-3 cm. Secondly, the nature of this problem is very much geometry, pressure, gas and operating point dependent, and therefore we will consider the specific examples where the pulse shaping data exists, namely the JET chamber of OPAL geometry [32], the TEC chamber [14] of the LEP3 experiment, and the Aachen University test [46].

We have made a specific prediction using the previously mentioned Monte Carlo program [9] that in the jet geometry operating with a fast gas, a 100 MHz digitizer is not fast enough to improve on the first electron timing (because of the ionization fluctuation effect). How does the situation look one year later when we have the first experimental results?

We have seen several experimental examples (table 5 provides an overall summary) in the previous chapters where eq. (2) provides rather close approximation to experimentally obtained results with the leading edge timing (even though

most practical tests do not trigger on the first electron). This means that for the leading edge timing the diffusion dominates the resolution at ~ 1 cm of drift distance and the ionization fluctuation effect represents a smaller contribution.

How is it in the case of the center of gravity timing? Let's first discuss the example of a jet chamber like OPAL, which operates with the "hot" fast gas 3% C_4H_{10} + 87.3% Ar + 9.7% CH_4 \sim JADE gas at 4 atm. The typical nonisochrony in this structure (5 mm wire to wire spacing) is shown in fig. 23. We can see that the diffusion is too small to smear this nonisochrony and at the same time the 100 MHz clock of FADC is too slow to provide several samples through a 2-3 mm "isochronous" central part of the sample. In fact for any number (≥ 2) of 10 ns bins we will be sensitive to the fluctuation in ionization statistics, which will shift the timing centroid significantly. One would expect that we reduce the sensitivity to this effect (and therefore improve the resolution) as we reduce the number of bins included in the timing algorithm. This is exactly observed in the data. Figure 24 indicates a time pulse reference method used in the FADC timing of the test with the OPAL full length prototype [15]. Table 4 shows the obtained resolution as a function of the method used. The best result is obtained if we use only two FADC bins for the reference timing. The measured 3-wire resolution is about 100 μm for 1 cm drift with the JADE gas at 4 atm. For comparison, if we use the eq. (2) we would expect for the first electron timing $\sigma_{\text{diffusion}} \sim 0.91\sqrt{\ln(4 \times 6 \times 3.0)} \times 250 \mu\text{m} \times 1/\sqrt{4} \sim 55 \mu\text{m}$ for 1 cm drift, and the eq. (3) for the center of gravity timing would give (a 20 ns window acceptance cut) $\sigma_{\text{diffusion}} \sim 1/\sqrt{(4 \times 15 \times 3)} \times 250 \mu\text{m} \times 1/\sqrt{4} = 10 \mu\text{m}$. This means that the experimental result is dominated by the ionization fluctuation effect and is worse than what we would expect from the leading edge timing. The second example comes from the Heidelberg test chamber [31], which has the same wire geometry but longer drift length. The results are shown in fig. 25 for various operating conditions. The fit to data is made using a function $\sigma^2 = \sigma_0^2 + \delta \cdot X$, where σ_0 contains mainly a contribution from the electronics and the ionization fluctuation effect. The fit indicates $\sigma_0 \sim 70\text{-}100 \mu\text{m}$ at 4 atm

and 135-160 μm at 2 atm depending on operating condition. Since the error in electronics contributes only 20-30 μm , one would again conclude that σ_0 is dominated by the ionization fluctuation effect (assuming that all other systematic contributions are negligible). It is interesting to predict the first electron leading edge capability for the best FADC data at 4 atm. Using fig. 26 we expect $\sigma_L \sim 155 \mu\text{m}$ for 1 cm of drift at $E/p \sim 0.47$. Using the eq. (2) we expect $\sigma_{\text{diffusion}} \sim 0.91/\sqrt{\ln(4 \times 6 \times 3)} \times 155 \mu\text{m}/\sqrt{4} \sim 34 \mu\text{m}$ for 1 cm drift, assuming that ~ 2 mm of track sample contributes to the leading edge timing in this particular geometry. It is interesting to point out that the best resolution is obtained at largest E . This is because of an improvement of the longitudinal diffusion as we increase E (see fig. 26) and the focusing effect mentioned earlier (see fig. 12). We have not yet mentioned so far another important variable and that is the gain on the wire. Both previous examples [15,31] operated at relatively lower gain ($< 5 \times 10^4$), because of the dE/dx application. In typical vertex chambers the gain is larger and one expects that some portion of the later arriving charge will be affected by the saturation effect. This will effectively tend to reduce the sample size for tracks reasonably perpendicular to the wires ($\theta \sim 0^\circ$), and one expects that the pulse waveform is more derived from the very early charge and therefore the centroid timing would approach the leading edge timing. If this is true one would expect some θ -dependence in the centroid timing resolution. Example of such application is the JADE experiment vertex detector [42]. They have achieved $\sim 100 \mu\text{m}$ resolution for 1 cm drift using the first two FADC timing bins in 50% Ar + 50% C₂H₆ gas at 1 atm. This is compatible with the expectation based on the eq. (2) for the first electron timing since the $\sigma_L(1 \text{ electron}) \sim 200 \mu\text{m}$ in this particular gas at 1 kV/cm, 1 cm drift and 1 atm. We see that the centroid timing will approach at best the leading edge timing at high gains in the fast gas.

One can ask the question under what condition we would improve the first electron timing in the jet chamber operating with the fast gas. Figure 27 shows the various simulated resolution results if we assume infinitely fast electronics capable of recording the arrival time of every electron [9]. We can see that the

center of gravity timing improves the first electron resolution only if we average over electrons in the near-isochronous central part of the sample (see fig. 23). As we average over larger parts of the sample (wider time window cut) the center of gravity is disturbed by the fluctuations in ionization statistics coupled with the nonisochrony of the charge collection. As we increase the pressure the diffusion gets smaller and the apparent isochronous part is even smaller requiring smaller timing cut. If we had ~ 1 GHz digitizer we would have a somewhat similar situation as in the TEC chamber we will discuss next, i.e. we would not detect every electron but instead have several samples through the average charge in the isochronous part of the fig. 23. With approximate cuts one could isolate this part of the signal and one would still expect an improvement over the first electron timing. One can express it differently, a 200 MHz digitizer would provide better resolution than ~ 100 MHz one, because we can further reduce the sample size through the timing cut.

How is it now in the TEC chamber [14]? Figure 28(a) shows details of the electrostatics of the charge collection. Figure 28(b) describes the approximately isochronous behavior in this chamber. We can see that it is not isochronous, but the nonisochrony affects only a small part of the track sample reducing the probability to have the ionization there. More important, the diffusion smears the charge to the point that we can consider that most of the track sample is isochronous. Finally, the speed of the 100 MHz digitizer is a good match to the low drift velocity providing 3-5 samples through the isochronous part of the sample. We would then expect that the center of gravity has a better chance to improve the leading edge timing. Figure 29(b) indicates a comparison of the leading edge timing with the center of gravity technique. Unfortunately this measurement is not yet conclusive evidence because the threshold for the leading edge timing was set apparently rather high (~ 6 electrons) [33]. For the first electron timing we would expect $\sigma_{\text{diffusion}} \sim 0.91/\sqrt{\ln(2 \times 6 \times 3.0)} \times 100 \mu\text{m}/\sqrt{2} \sim 34 \mu\text{m}$ for 1 cm of drift at 2 atm. On the other hand, the diffusion contribution using the center of gravity timing [eq. (3)] is $\sigma_{\text{diffusion}} \sim$

$1/\sqrt{2 \times 6 \times 3}) \times 100 \mu\text{m}/\sqrt{2} \sim 11 \mu\text{m}$ for 1 cm of drift. Since the electronics gives a small contribution [33] we would conclude that other systematic effects including the finite ionization statistics, the finite speed of the digitizer, the diffusion near the anode wire, etc. still contributed the large contribution to their measured results. This is also visible if we use their fit to the data $\sigma^2 = \sigma_0^2 + \delta \cdot X$ where $\sigma_0 = 19 \mu\text{m}$. Because σ_0 is so small it is harder to determine the dominating term in this particular case. Anyway, our conclusion is that both timing techniques will be approximately equivalent for ~ 1 cm drift distance. The real benefit of the center of gravity timing is expected through far larger drift distances ($> 2\text{-}3$ cm) where the diffusion will cause the leading edge resolution to be worse.

Final example comes from the Aachen University test [46], where the cylindrical cell was tested with the cool gas 80% CO_2 + 20% C_4H_{10} and using both the leading edge and 100 MHz flash ADC electronics. Figure 32 shows the results. One can see that the leading edge timing is significantly better for small distances from the anode wire and both methods yields similar results further away from the wire. The explanation is rather simple. For a cylindrical cell where the field E is approximately proportional to $1/r$, and for a cool gas like CO_2 with v_{drift} proportional to E , one expects that the drift velocity is rapidly changing with the distance from the anode wire – see fig. 32(a). Far from the wire, the charge collection is more isochronous compared to small impact parameters, where the velocity begins to be too large. The 100 MHz clock, similarly like in our first example, is too slow for small impact parameters and the ionization fluctuations begin to dominate the FADC timing.

6. The “Ultimate” Design?

All arguments in this chapter are based on the computer simulation of the problem. As we said earlier the mesh represents the ideal electrostatic boundary in the TEC chamber. However, it is difficult to implement in practice for larger chamber designs. Figure 33 shows several alternatives to the mesh solution as simulated by the author. The basic wire geometry and the voltages were kept the same as in fig. 28(a), however, the mesh was replaced either with a foil or a grid of wires. The simulation was performed for 92% CO₂ + 8% C₄H₁₀, $E \sim 1.1$ kV/cm, pressure $p = 2$ atm and the diffusion parametrization according to fig. 2. For clarity of the picture, the clustering was switched off and the amount of ionization was artificially increased. The question is then what kind of effect these geometrical solutions have on the isochrony of the charge collection. Figure 33(a) shows a case where the foils are separated by a 1 mm gap. One can see that in this case there is a nonisochrony due to a ripple in the electrostatic field caused by the 1 mm gap. In fig. 33(b) we tried to remove this problem by placing one wire in the middle of the gap. In fig. 33(c) we used a 1 mm grid. In this case one obtains the worst nonisochronous condition, which will tend to create a tail in the drift pulses. The case of fig. 33(b) is clearly the best. For a drift distance larger than 1 cm the diffusion makes this geometry truly isochronous. According to our simulation one expects a 3σ double track separation of about 80-150 μm for ~ 1 cm drift. If we incline the track by 10° this quantity will double. Figure 34 shows a version of what one could consider an “ultimate” design of the vertex chamber. As we can see it is a combination of the TEC concept, and the charge restricting and the charge focusing geometry.

As we said the diffusion will smear the nonisochrony after a certain drift distance. This distance is pressure dependent. For instance, at 2 atm we will not see much difference in width of the drift time distributions between the designs on fig. 33 after a drift distance of about 2-3 cm. Figure 35 shows the drift time distributions at 4 atm for various designs and several drift distances. Figure 36

shows the same but for tracks inclined by 10° with respect to the anode plane. One can see that at this pressure and a drift distance of 22 mm, the design (a) has FWHM of the drift time distribution typically 20-30% smaller compared to the design (d) of fig. 35 [fig. 35(a) \equiv fig. 33(b)]. This will have a consequence on the multiple hit capability. How does it affect the resolution? We have performed the resolution study on these two designs (a) and (d) of fig. 35, with infinitely fast electronics as well as with realistic pulses generated with a realistic primary ionization, and convoluting the drift time distribution with a response of an amplifier and one zero pole filter. The results of this study are summarized in table 6. We conclude that the centroid timing with the infinitely fast electronics capable of detecting each electron separately follows approximately the eq. (3), however, the centroid timing with the realistic pulses and a 100 MHz digitizer is worse, and it is about equivalent to the first electron timing for 12 mm drift distance. This is even true for the near ideal isochronous design of fig. 33(b). We interpret this as a possible indication that even for the slow gas the 100 MHz digitizer is not fast enough to provide a true representation of the pulse shape and therefore we do not achieve the ultimate resolution as given by eq. (3). This points to a need to increase the speed of the digitizers. We have tried to increase the speed of the digitizer to 500 MHz in the same study with the design of fig. 33(b). Using the realistic drift pulses, which included avalanche fluctuations, we have not managed to improve the resolution significantly compared to the leading edge timing. Nevertheless, we believe that the case should be tried experimentally because at this level one should not trust the computer program completely. The chamber should operate at a very low gas gain with a low noise high gain electronics to be able to use all electrons arriving to the wire. If one would achieve the resolution as predicted by eq. (3), we would directly compete with the solid state devices! There is certainly enough primary ionization produced at 4 atm to expect this. The question is what the electronics does with it. One will have to find a correct compromise between the amplifier speed and the digitization speed. Application for this? – The innermost layers of the vertex chamber.

7. Conclusion

- (a) For applications where an excellent resolution, multiple track resolution, insensitivity to angles and insensitivity to the space charge effects is required, I would consider the TEC chamber with the restricting curtains. The challenge here is to come up with the best possible design of the restricting curtains. It can be operated either with the "cool" or "hot" gases depending on the environment, and even with simple leading edge timing and multiple hit "switchyard" electronics one can achieve very good results. For applications where the multiple track separation is not important the simple jet chamber or the tube design will perform well. The radial drift chamber is still in a prototyping stage.
- (b) More work should and will be done on an improvement of the charge collection focusing techniques, either through a suitable choice of a gas or using electrical fields (or both). Here the aim is mainly to improve the double hit capability.
- (c) If the choice is a "cool" gas, much more work should go to studies of the systematic effects.
- (d) For the fast gases, lower gains and drift distances less than 1-2 cm, a simple leading edge timing will provide better resolution than existing 100 MHz waveform digitizers. At high gains the centroid timing will approach the leading edge timing. In the case of slow gases and depending on exact charge collection geometry, the 100 MHz digitizer will provide comparable results to the leading edge technique for small drift distances. By the leading edge we mean the ~ 1 electron threshold timing. Certainly one should not expect a drastic improvement according to eq. (3), unless we create a truly isochronous geometry, find some trick to correctly reproduce the drift pulses in a process of digitization and learn more about details of remaining systematic errors.

- (e) For larger distances (2-3 cm) the pulse shape timing will definitely be better than the leading edge timing because the sensitivity to diffusion is reduced.
- (f) To achieve resolution better than 40 μm for 1 cm drift, one has to pressurize the gas to 2-4 atm. To improve the resolution through an improvement of the collection optics is a much slower way to gain.

ACKNOWLEDGEMENTS

We would like to thank Professor J. Heintze for discussions of several topics in this paper. We also appreciate comments about this subject by Dr. G. Viertel and Professor A. Wagner. We also thank J. Fehlmann for running the program to predict the diffusion parameters for several gas mixtures (4).

REFERENCES

- [1] G. Charpak and F. Sauli, CERN-EP/84-35, submitted to Annual Reviews of Nuclear Sciences.
- [2] See for example H.S.W. Massey and E.H.S. Burshop, *Electronic and Ionic Impact Phenomena*, Oxford, 1969.
- [3] B. Schmidt, Heidelberg diploma thesis, 1980.
- [4] J. Fehlmann, J.A. Paradiso and G. Viertel, "WIRCHA" Program Package to Simulate Drift Chambers, ETH Zürich, 1983.
- [5] W. Farr, J. Heintze, K.H. Hellenbrand and A.H. Walenta, Nucl. Instrum. Methods 154 (1978) 175-181.
- [6] H. Cramer, *Mathematical Methods of Statistics*, Princeton University Press, 1966, p. 374.
- [7] J. Va'vra and L. Roberts, *DRIFT Program*, SLAC, 1982.
- [8] C. Prescott, SLD Group, Using a program of ref. [7].
- [9] J. Va'vra, SLAC-PUB-3131, presented at the 2nd Pisa Meeting on Advanced Detectors, Castiglione, 1983; and Nucl. Instrum. Methods 225 (1984) 445.
- [10] F. Lapique and F. Piuz, Nucl. Instrum. Methods 175 (1980) 297.
- [11] S. Bobkov *et al.*, CERN-EP/83-81.
- [12] D. Bettoni and A. Rudge, NA34 Internal Note #48.
- [13] D. Bettoni *et al.*, NA34 Experiment Note, presented at International Conference on High Energy Physics, Brighton, 1983.
- [14] Aachen-Siegen-Zürich Vertex Chamber Group, presented at S. Miniato Meeting on Future High Energy Machines, Florence, Italy, 1984.
- [15] H. Burckhart, J. Va'vra, K. Zankel, U. Dudziak, D. Friedrich, O. Schaile, P. Lennert and P. Igo-Kemenes, CERN EF/85-11.

- [16] H. Drumm *et al.*, Nucl. Instrum. Methods 176 (1980) 333-344.
- [17] J. Va'vra and L. Roberts, SLC Note #31, SLAC, 1982.
- [18] E.R. Belau, W. Blum, Z. Hajduk and T.W.L. Sanford, Nucl. Instrum. Methods 192 (1982) 217-221.
- [19] J. Va'vra, Nucl. Instrum. Methods 217 (1983) 322-326.
- [20] R.A. Boie, A.T. Hrisoho and P. Rehak, Nucl. Instrum. Methods 192 (1982) 365-374.
- [21] SLD Design Report, SLAC, 1984.
- [22] J. Va'vra, SLAC-PUB-2984 (1983).
- [23] OPAL Vertex Chamber (Rutherford Lab. Electronics).
- [24] SLD Central Detector Group, presented by H. Lynch at S. Miniato Meeting on Future High Energy Machines, Florence, Italy, 1984.
- [25] J. Jaros, proceedings of the International Conference on Instruments for Colliding Beam Physics, SLAC-250, 1982.
- [26] ARGUS Vertex Detector Group, presented at S. Miniato Meeting on Future High Energy Machines, Florence, Italy, 1984.
- [27] A.H. Walenta, proceedings of the International Conference on Instruments for Colliding Beam Physics, SLAC-250, 1982.
- [28] F. Villa, Nucl. Instrum. Methods 217 (1983) 273-276.
- [29] K.H. Hellenbrand, Heidelberg diploma thesis, 1980.
- [30] G. Schultz and J. Gresser, Nucl. Instrum. Methods 151 (1978) 413.
- [31] L. Smolik, Heidelberg diploma thesis, 1984; presented by J. Heintze at S. Miniato Meeting on Future High Energy Machines, Florence, Italy, 1984.
- [32] The OPAL Detector Technical Proposal, CERN/LEPC/83-4 LEPC/P 3.
- [33] Private communication with Dr. G. Viertel and J. Fehlmann.

- [34] R.D. Hake and A.V. Phelps; Phys. Rev. 133A (1964) 375.
- [35] General overview can be found in A. Peisert and F. Sauli, CERN 84-08 (1984).
- [36] G. Schultz and J. Gresser, Nucl. Instrum. Methods 151 (1978) 413.
- [37] A. Breskin, G. Charpak and F. Sauli, Nucl. Instrum. Methods 136 (1967) 497.
- [38] D. Bettoni *et al.*, presented at S. Miniato Meeting on Future High Energy Machines, Florence, Italy, 1984.
- [39] V. Palladino and B. Sadoulet, Nucl. Instrum. Methods 128 (1975) 323.
- [40] Compilation taken from Proceedings of the SLC Workshop on Experimental Use of the SLAC Linear Collider, SLAC-247, 1982.
- [41] This concept was originally used at 1 atm by the HRS experiment at SLAC. The MAC test results published in SLAC-PUB-3390, 1984.
- [42] A. Wagner, private communication.
- [43] M. Matoba *et al.*, IEEE Trans. NS-32 (1985).
- [44] H.F.W. Sadrozinski, Santa Cruz University preprint, SCIPP-84/28.
- [45] D. Smith, private communication.
- [46] V. Commichau *et al.*, Aachen University preprint, PITHA 84-34.
- [47] J. Jaros, private communication.
- [48] M. Basile *et al.*, CERN-EP/85-40.
- [49] J. Huth and D. Nygren, TPC-LBL-85-7.
- [50] C.C. Young *et al.*, SLAC-PUB-3782.
- [51] J. Fischer, A. Hrisoho, V. Radeka and P. Rehak, BNL 35819 (1985), submitted to Nucl. Instrum. Methods.

- [52] R. Bouclier, G. Charpak, L. Ropelewski, J.C. Santiard, N. Solomey and F. Sauli, IEEE Trans. Nucl. Sci. (1985).

Table 1

Type of Cell	Pressure	Gas	Type of Electronics	Resolution (σ /Drift Dist.)	Experiment	Type of Measurement
Cylindrical	1 atm	hot	Leading Edge	$\geq 80 \mu\text{m}/5 \text{ mm}$	Mark II	Physics [25]
	1.5-2 atm	cool	Leading Edge	$40-100 \mu\text{m}/5 \text{ mm}$	ARGUS	Physics [26]
	4 atm	hot	Leading Edge	$\gtrsim 30 \mu\text{m}/2 \text{ mm}$	MAC	Physics [41]
	1 atm	cool	Leading Edge	$\gtrsim 30 \mu\text{m}/5 \text{ mm}$	-	Test [46]
Jet	4 atm	hot	Leading Edge	$23 \mu\text{m}/4 \text{ mm}$	-	Test [18]
	4 atm	hot	Leading Edge	$< 55 \mu\text{m}/8 \text{ mm}$	NA27, CERN	Test
	6.1 atm	hot	Leading Edge	$22 \mu\text{m}/2 \text{ mm}$	-	Test [19]
	4 atm	hot	100 MHz FADC	$70-80 \mu\text{m}/1 \text{ cm}$	OPAL	Test [15]
	1 atm	cool	Leading Edge	$\sim 60 \mu\text{m}/1 \text{ cm}$	SLD #1	Test [35]
	3 atm	hot	Leading Edge	$\sim 40-50 \mu\text{m}/1 \text{ cm}$	UA-1	Test [45]
Time Expansion (TEC)	2 atm	cool	Leading Edge	$< 40 \mu\text{m}/1 \text{ cm}$	LEP3	Test [14]
			100 MHz FADC	$\sim 30 \mu\text{m}/1 \text{ cm}$	-	
	2.7 atm	cool	Leading Edge	$\sim 30 \mu\text{m}/1 \text{ cm}$	-	Test [48]
Sample Length Restricting	4 atm	cool	Leading Edge	$\leq 30 \mu\text{m}/1 \text{ cm}$	-	Test [11]
	1 atm	cool	Leading Edge	$\sim 65 \mu\text{m}/1 \text{ cm}$	NA34, CERN	Test [38]
Special Focusing	1 atm	cool	Leading Edge	$\sim 45 \mu\text{m}/1 \text{ cm}$	SLD #2	Test [50]
	1 atm	cool	Leading Edge	$\sim 65 \mu\text{m}/1 \text{ cm}$	NA34, CERN	Test [13]
	3 atm	cool	Leading Edge	$\sim 35 \mu\text{m}/1 \text{ cm}$	Mark II	Test [47]

Table 2

Type of Chamber	Drift Length	Average Drift Velocity	Total Drift Time	Spatial Error Due To		
				Error In v or t (1/1000)*	Error In E (1/1000)*	Error In Gas Density (1/1000)*
"Slow" Drift	1 cm	5 $\mu\text{m}/\text{ns}$	2 μsec	10 μm	10 μm	10 μm
"Fast" Drift	1 cm	30-50 $\mu\text{m}/\text{ns}$	≤ 200 ns	10 μm	5×10^{-3} μm	~ 0

* - Assumption

Table 3

Quantity	"Fast" Drift	"Slow" Drift (with "cool" gas)	"Slow" Drift (with "low" E)
Gas	90% Ar + 10% CH ₄	90% CO ₂ + 10% C ₄ H ₁₀	90% Ar + 10% CH ₄ + Methylal
Pressure	4	2	2
E	4 kV/cm	1.2 kV/cm	200 V/cm
μ^+	1.9 cm ² /Vsec	1.1 cm ² /Vsec	1.9 cm ² /Vsec
T^+ (1 cm gap)	1.3×10^{-4} sec/atm	7.6×10^{-4} sec/atm	2.6×10^{-3} sec/atm
ϵ	$\sim 0.5^*$	$\sim 0.1^*$	$\sim 0.1^*$
ρ^+	2.6×10^{-13} C/cm ³ . atm	3×10^{-13} C/cm ³ . atm	1×10^{-12} C/cm ³ . atm
$ \Delta E/E _{\max}$	4×10^{-4}	1.4×10^{-3}	28×10^{-3}
ΔX	$\sim 0 \mu\text{m}$	$\sim 15 \mu\text{m}$	$\sim 280 \mu\text{m}$

* - Assumption

Table 4

Timing Method	σ [ns] (1 cm of drift)	σ [μm] (assume 50.4 $\mu\text{m}/\text{ns}$)	Relative Accuracy
Ref. Pulse – 2 FADC Bins (equal weight)	2.0	101	1.00 ± 0.01
Ref. Pulse – 3 FADC Bins	2.3	116	1.15
Ref. Pulse – 4 FADC Bins	2.4	121	1.18
Ref. Pulse – 5 FADC Bins	2.6	131	1.30
Ref. Pulse – 6 FADC Bins	2.8	141	1.42
Ref. Pulse – 10 FADC Bins			
(a) Weighted: 9,6,3,2,6*1	2.3	116	1.13
(b) Weighted: 5,4,3,2*1,5*0	2.3	116	1.16
(c) Weighted: 20,5,3*1,5*0	2.2	111	1.08
Maximum Peak Method	5.1	257	–
Center of Gravity (average over 200 ns)	4.0	202	–
Spline Fit	3.0	151	–

Note:

1. Best algorithm for short drift distances (≤ 3 cm) is a simple reference timing with two equally weighted FADC bins.
2. Further reduction in resolution of about 0.2 ns (10 μm) can be obtained if the cross-talk compensation would be implemented.

Table 5

Type of Cell	Pressure (atm)	Effect Sample Size ^d (mm)	ηNnp (#)	$F = \frac{0.91}{\sqrt{\ln(\eta Nnp)}}$	Average Drift (cm)	σ_L (1 electron) at 1 atm ($\mu\text{m}/\sqrt{\text{cm}}$)	$\sigma_{\text{diffusion}}$ Eq. (2) (μm)	$\sigma_{\text{experiment}}$ (μm)
Jet [18]	4.0	~ 0.8	33	0.49	0.4	120	19	23
Micro-Jet [19]	6.1	~ 0.2	11	0.59	0.2	≥ 125	16 ^c	22
Jet [24]	1.0	~ 1.0	9	0.61	1.0	80	49	60
Sample Restrict [11]	4.0	~ 0.8	29	0.50	1.0	70	17	30
Special Focus [13]	1.0	~ 1.5	14	0.56	1.0	70	42	60
TEC [14]	2.0	~ 2.0	36	0.48	1.0	100	34	40 ^e
Jet [45]	3.0	~ 0.6	17	0.54	0.5	200	44	40-50

Note:

- (a) In calculation assume the first electron timing.
- (b) The measurements used the low threshold leading edge timing.
- (c) We cannot use the eq. (2) in this particular case because we have not kept E/p constant as we change the pressure p . We used instead $\sigma_{\text{diffusion}} = F \times \sigma_L^o(\text{1electron}) \times \sqrt{(E/p)^\alpha X/E}$, where σ_L^o is normalized to 1 kV/cm, 1 atm and 1 cm of drift; $E = 14.6 \text{ kV/cm}$, $\sigma_L^o = 130 \mu\text{m}/\sqrt{\text{cm}}$.
- (d) The effective sample size is estimated from the Monte Carlo program (see fig. 10).
- (e) The test had an equivalent threshold of ~ 6 electrons for the leading edge timing.

Table 6

Timing Method	Resolution (microns)			
	Design (a)		Design (d)	
	0 deg	10 deg	0 deg	10 deg
(1) First electron timing with infinitely fast electronics	20 ± 3	34 ± 3	25 ± 2	32 ± 3
(2) Centroid timing with infinitely fast electronics (average over the first 100 ns only)	7 ± 1	14 ± 2	12 ± 1	13 ± 1
(3) Leading edge timing with the realistic pulses (threshold $\sim 2-3\%$ of the average amplitude)	20 ± 3	48 ± 4	29 ± 2	36 ± 3
(4) Centroid timing with the realistic pulses and 100 MHz digitizer (use the simple centroid timing)	20 ± 1	27 ± 2	36 ± 3	43 ± 3

Note:

1. Simulation performed from 4 atm pressure, 12 mm drift distance, 92% CO₂ + 8% C₄H₁₀ gas and the drift velocity $v = 4.0-4.2$ microns/ns.
2. The examples correspond to figs. 35(a) and (d), 36(a) and (d); [fig. 33(b) \equiv fig. 35(a)].
3. The angle refers to an angle of the track and the anode plane.

FIGURE CAPTIONS

1. Characteristic energy, drift velocity and diffusion (for 1 cm of drift and 1 atm pressure) in CO₂ as a function of the electric field [34].
2. Diffusion for 1 cm drift and 1 atm pressure as a function of the electric field [11].
3. Characteristic energy as a function of the electric field in hot gas mixtures [39].
4. Diffusion for 1 cm drift and 1 atm pressure for typical hot gases [40].
5. Measured transverse and longitudinal diffusion in JADE gas [3].
6. Calculated transverse and longitudinal diffusion in 90% Ar + 10% C₄H₁₀ for 1 cm drift and 1 atm [4].
7. Influence of gas pressure on localization accuracy of a drift chamber [5].
8. The computer simulation of the drift pulses caused by particles in the micro-jet chamber [9].
9. Examples of the charge collection in typical drift chambers.
10. Schematic view of (a) isochronous and (b) nonisochronous charge collection with indication of the effective sample length.
11. Schematic view of the nonisochronous charge collection in the jet chamber operating with 90% Ar + 10% C₄H₁₀ gas at 1 atm and $B = 10$ kG [9].
 - (a) The effect of diffusion and clustering on the drift pulse randomness (avalanche fluctuation and electronics response included).
 - (b) The effect of the impact parameter (0 and 6 mm).
 - (c) The effect of the angle of the track ($B = 0$ kG) [17].
12. The effect of the drift velocity behavior on the isochrony of the jet chamber. The drift time distribution gets narrower for the gas #2 [17].

13. Cell configuration and measured spatial resolution of a simple wire as a function of gas pressure in a high precision jet chamber [18].
14. Cell configuration and measured spatial resolution of a single wire as a function of impact parameter in a micro-jet chamber (90% Ar + 10% C₄H₁₀ gas used) [19].
15. Spatial resolution obtained in the SLD prototype #1 (simple jet chamber) in 92% CO₂ + 8% C₄H₁₀ at 1 atm using the leading edge timing [24]. The solid line is a fit of the form $\sqrt{C_0^2 + C_1^2 X}$ where $C_0 = 0.081$ and $C_1 = 63.5 \mu\text{m}\cdot\text{cm}^{-1/2}$.
16. Spatial resolution in ARGUS vertex chamber [26].
17. Example of charge restricting geometry:
 - (a) The prototype configuration.
 - (b) Spatial resolution using a leading edge timing as a function of impact parameter.
 - (c) Spatial resolution of the second track as a function of a distance from the first track.
 - (d) Efficiency to find the second track as a function of a distance from the first track.
 - (e) Future plan [11].
18. Example of a charge focusing geometry:
 - (a) Drift cell configuration.
 - (b) Lines of equal drift time.
 - (c) Measured spatial resolution in this cell.
 - (d) The measured spatial resolution in cell as in fig. 17(e) with 2 mm restricting gap [13].
19. (a) Example of a charge focusing geometry in the SLD prototype #2 [21,50].

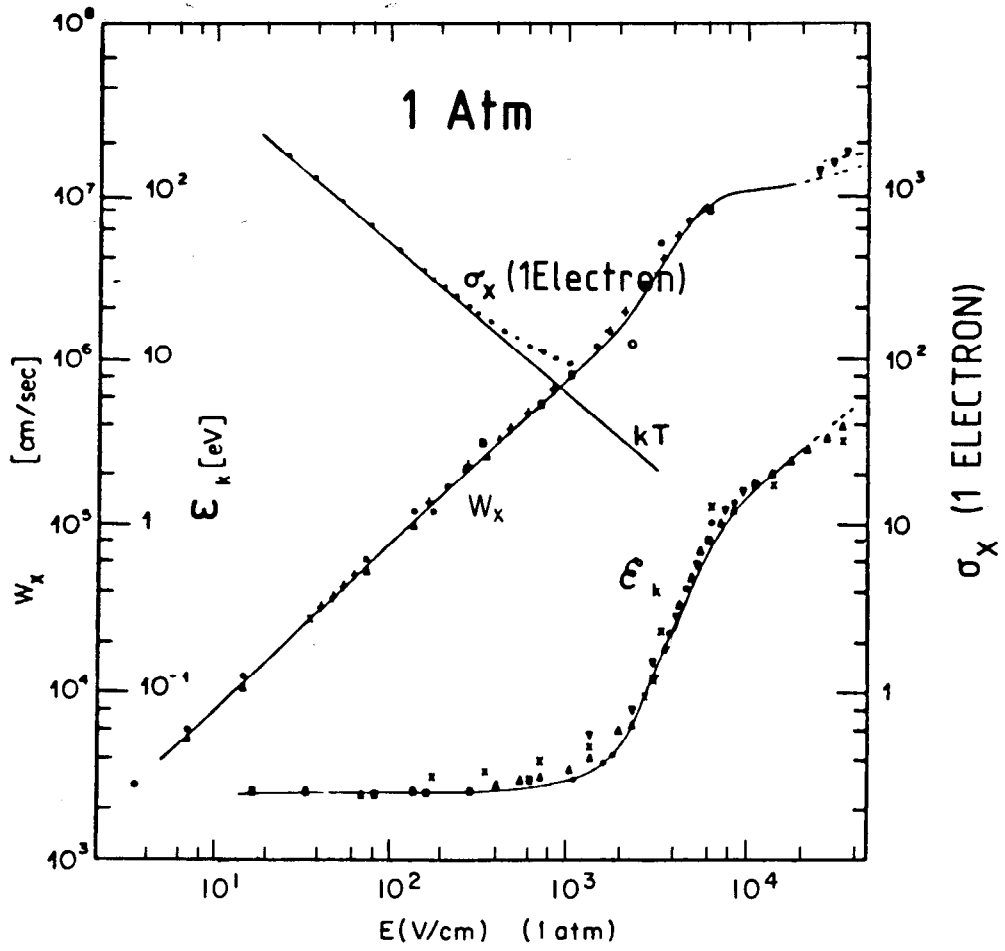
(b) Measured resolution in 92% CO₂ + 8% C₄H₁₀ at 1 atm using the leading edge timing. The smooth curve is the prediction of a computer Monte Carlo simulation [8].

20. Time expansion chamber prototype [14].
21. Sensitivity of a constant k for various gas mixtures ($\Delta v/v = k(\Delta E/E)^2$) [29].
22. Field dependence of the relative temperature variation of drift velocity, as computed gases [36] and measured for various gases (· - 90% Ar + 10% CH₄ [1], X - Ar, C₄H₁₀, methylal [37]).
23. Schematic view of nonisochronous behavior of jet chamber like OPAL.
24. The principle of the method of timing with the FADC using a reference pulse. The method minimizes a quantity

$$Q = \sum_{i=1}^N W_i \left[Y_i^{\text{REF}} - Y_i^{\text{FADC}} \right]^2 .$$

25. Measured spatial resolution using the FADC timing for various operating points as a function of drift distance in the OPAL prototype [31].
26. Calculated transverse and longitudinal diffusion in 90% Ar + 10% CH₄ for 1 cm drift and 1 atm [4]. Numbers correspond to various operating points of fig. 25-1.
27. The simulated timing resolution using a hypothetical infinitely fast electronics capable of digitizing every arriving electron in jet chamber with 4 mm wire spacing, 90% Ar + 10% C₄H₁₀ at 1 atm, $B = 10$ kG and 7.5 mm impact parameter [9].
28. (a) Lines of equal drift time in the time expansion prototype [14].
(b) the schematic view of nonisochronous behavior in this cell.

29. (a) Measured spatial resolution of the time expansion chamber prototype at 1 and 2 atm (FADC timing) [14].
(b) Measured spatial resolution of the time expansion chamber prototype for two timing methods (FADC and TDC timing). The TDC threshold corresponds to ~ 6 electrons [33].
30. Results from TEC test [48] using the dimethyl ether gas and the leading edge timing.
31. Principle of the radial drift chamber [49].
32. Results from the Aachen University test [46].
(a) Drift velocity as a function of a distance between the anode and the track.
(b) Measured resolution using the TDC and FADC techniques.
33. Isochronous behavior for various alternatives of the charge collection in the TEC chamber as simulated by author for 92% CO₂ + 8% C₄H₁₀, 2 atm and $E \simeq 1.1$ kV/cm [voltages and wire geometry the same as in fig. 28(a)].
(a) Charge restricting geometry using foils with 1 mm gap.
(b) Adding a wire into the middle of the gap, otherwise as point (a).
(c) 1 mm wire gap grid system.
34. Possible version of an "ultimate" design using the TEC concept, the charge restricting and the charge focusing geometry.
35. Drift time distributions for various designs and several drift distances for 92% CO₂ + 8% C₄H₁₀, 4 atm pressure and the drift velocity of about 4-4.2 $\mu\text{m}/\text{ns}$ (the amount of ionization artificially increased for greater clarity).
36. The same as fig. 35 but the track inclined by 10° in respect to the anode plane.



5182A6

↑
~2 kV/cm

Fig. 1

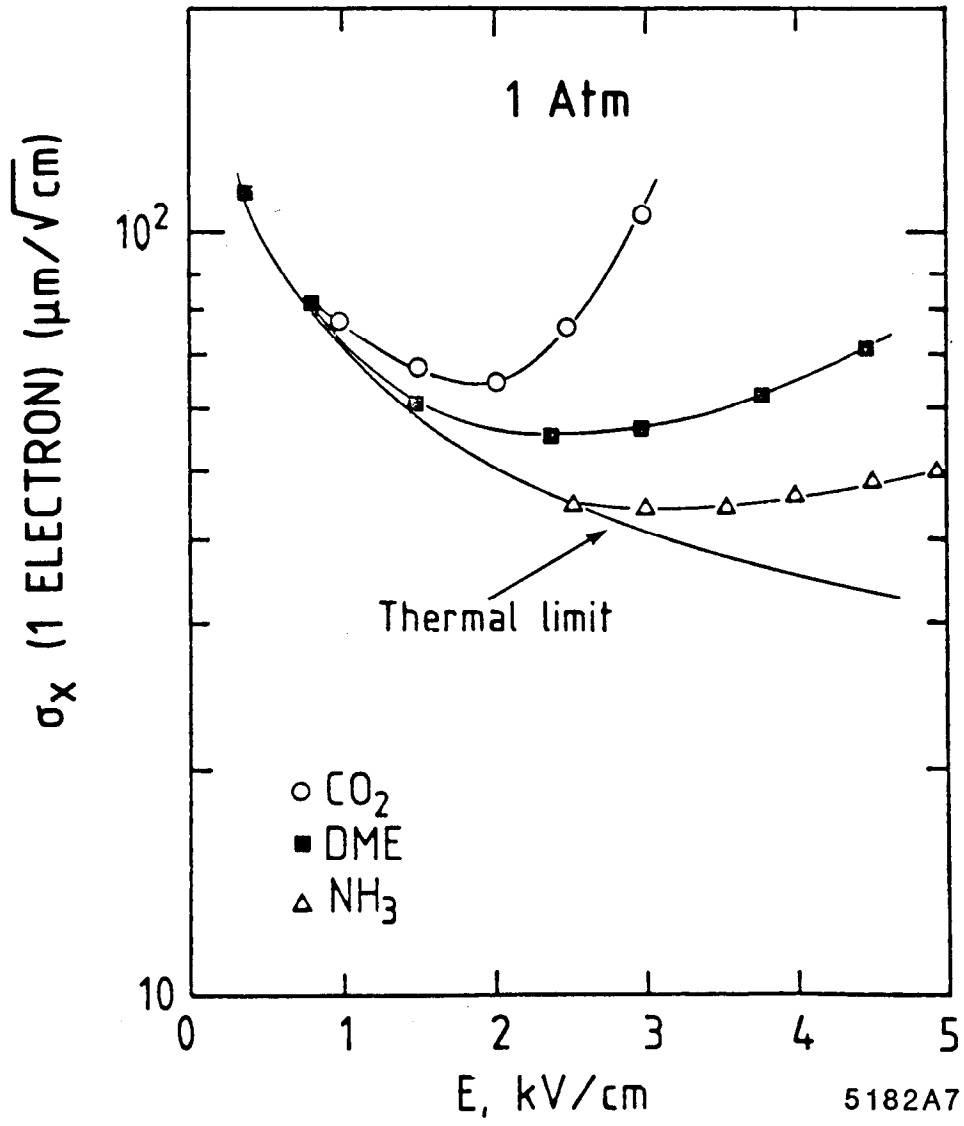


Fig. 2

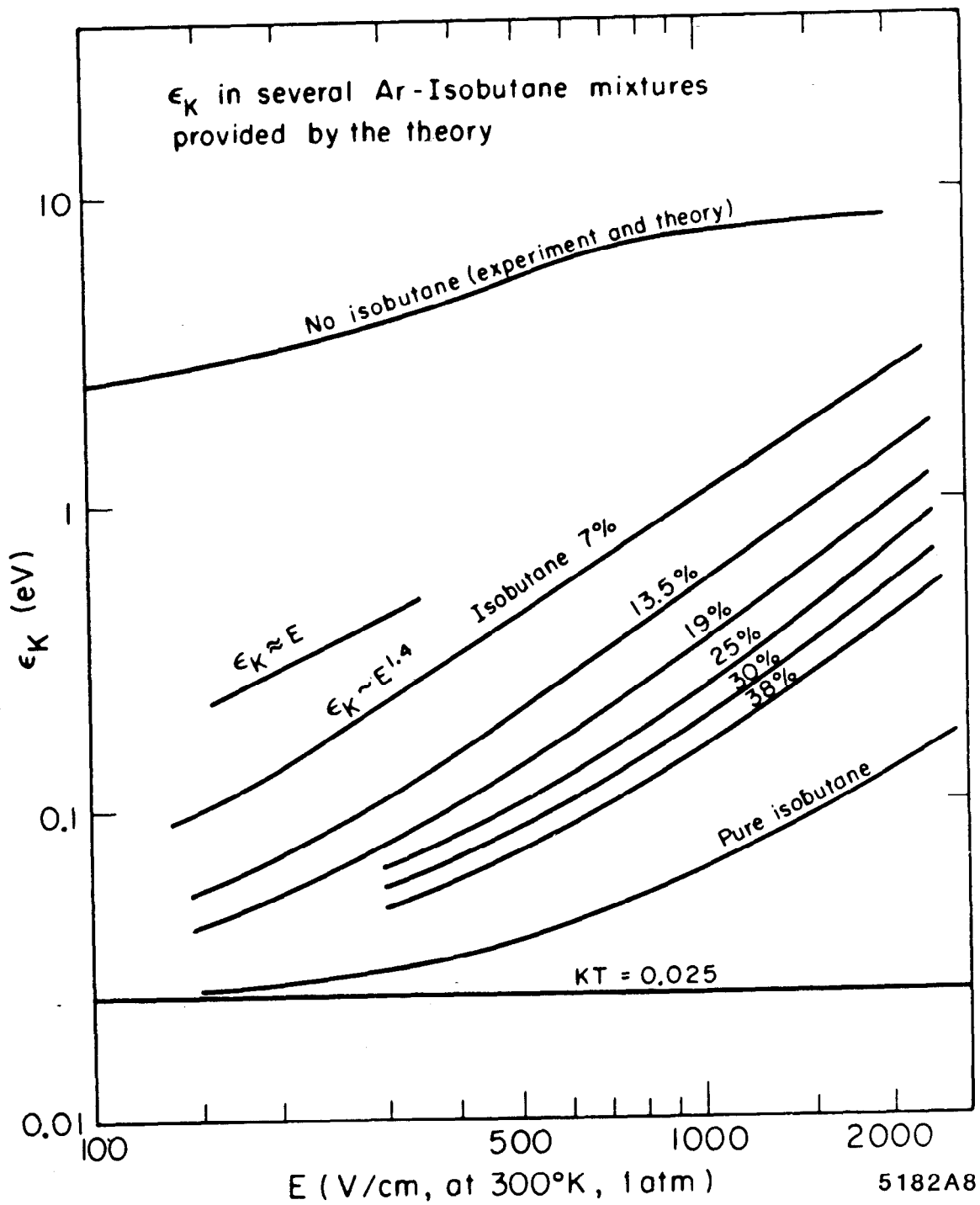


Fig. 3

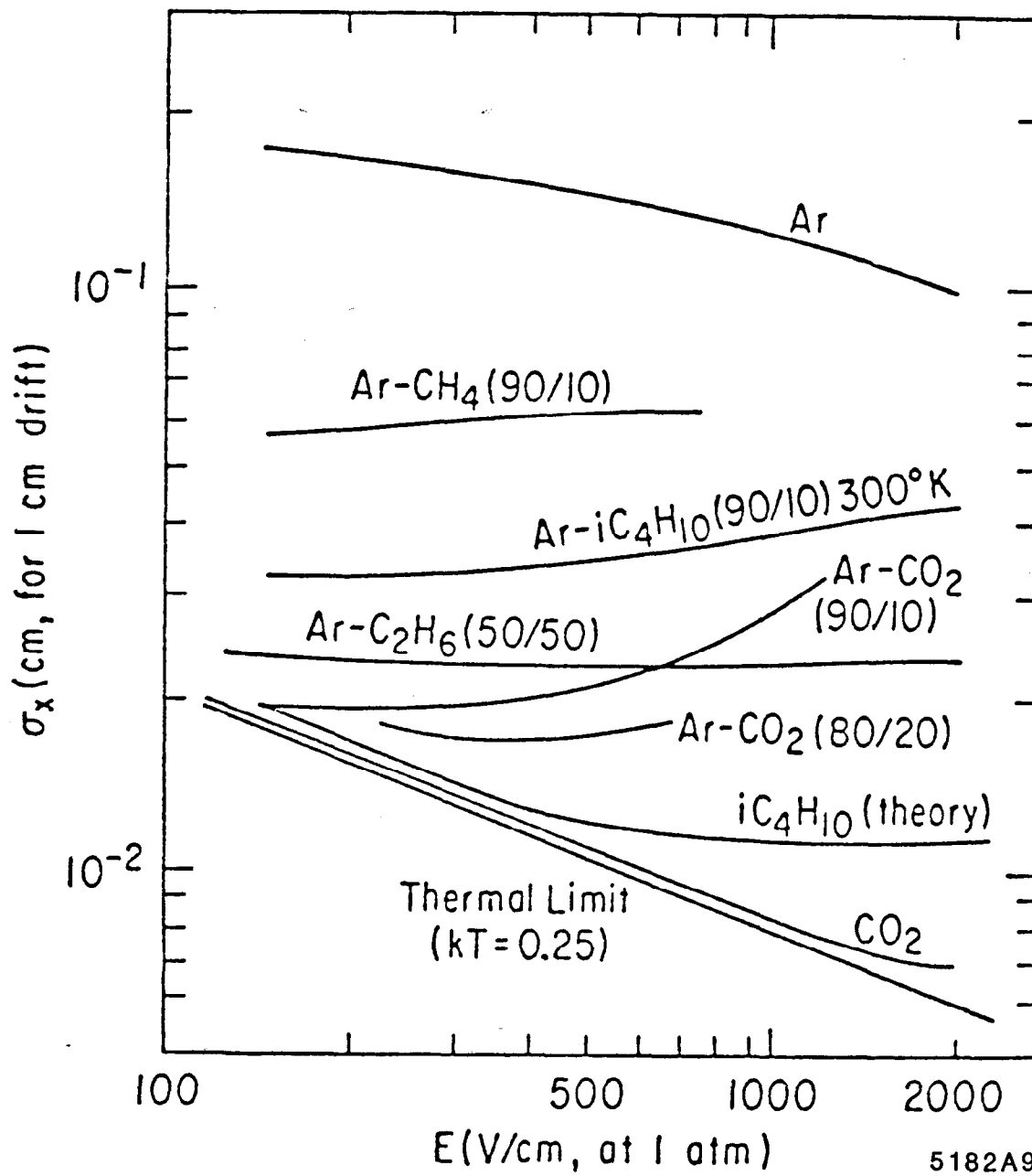


Fig. 4

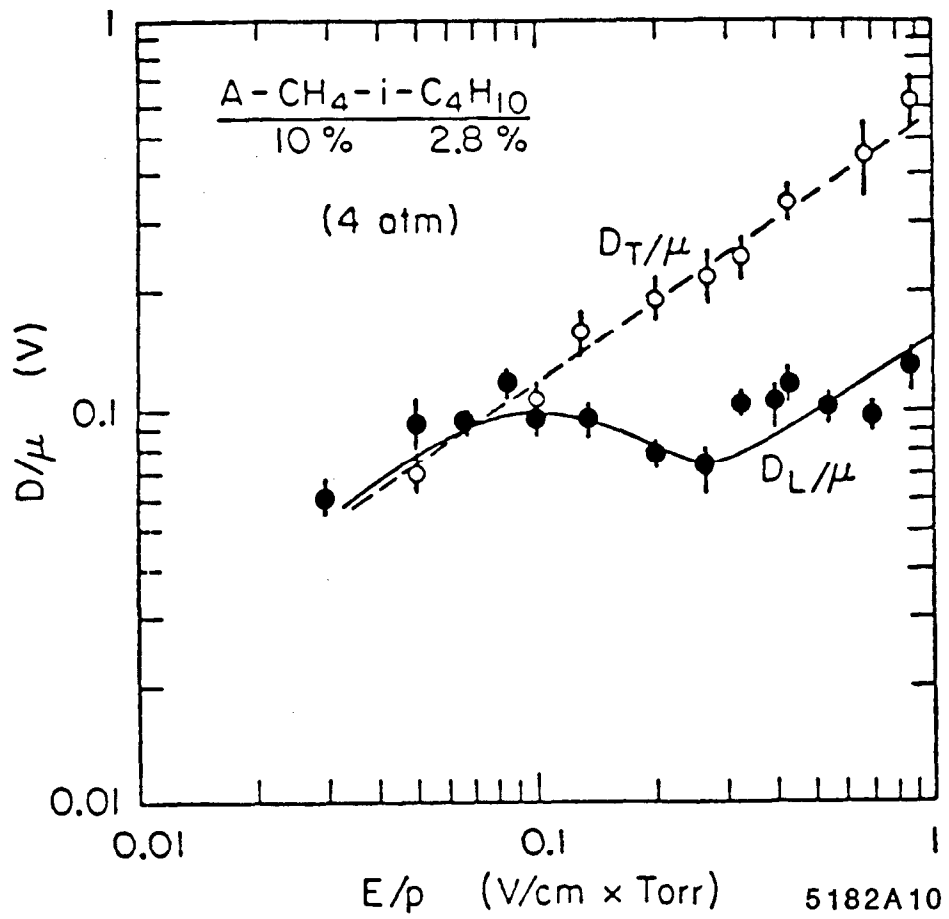


Fig. 5

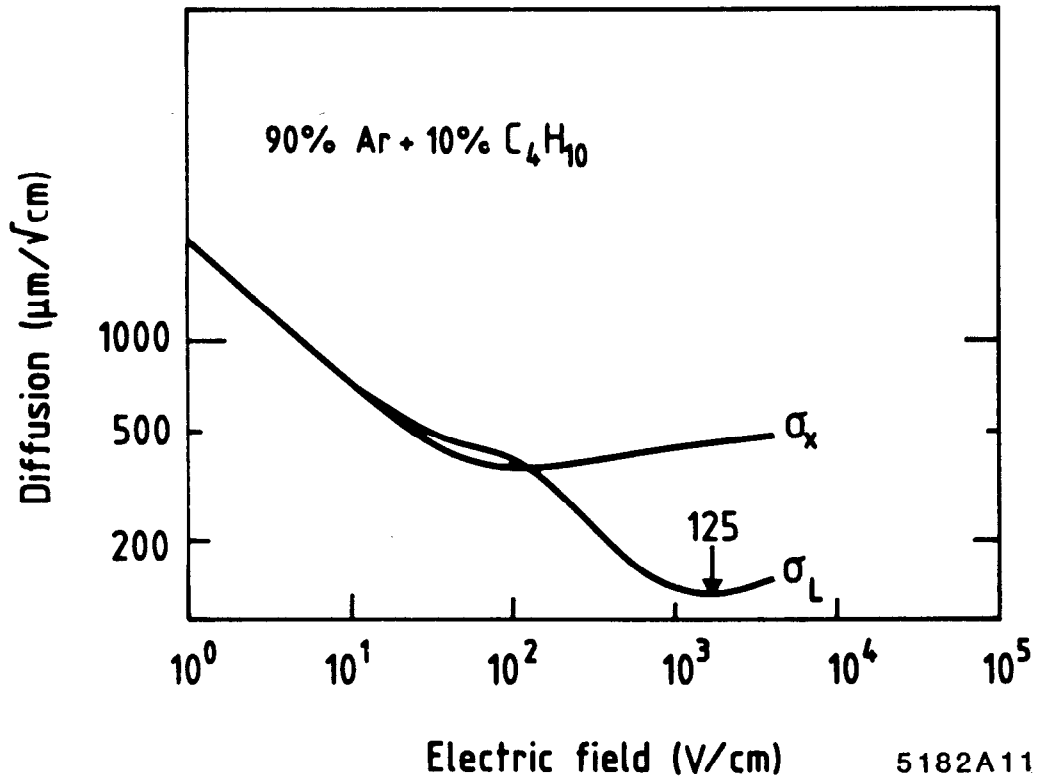


Fig. 6

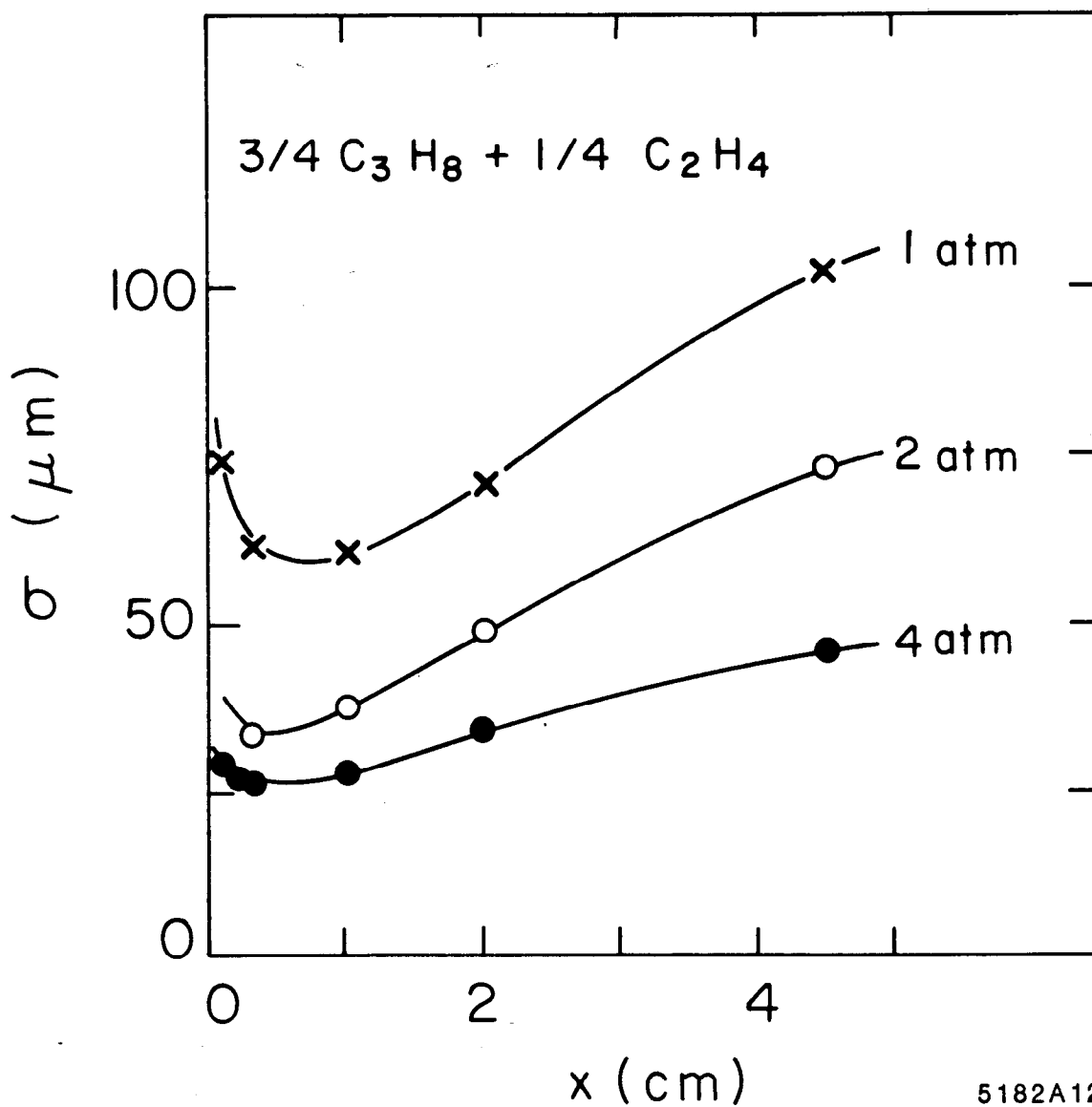


Fig. 7

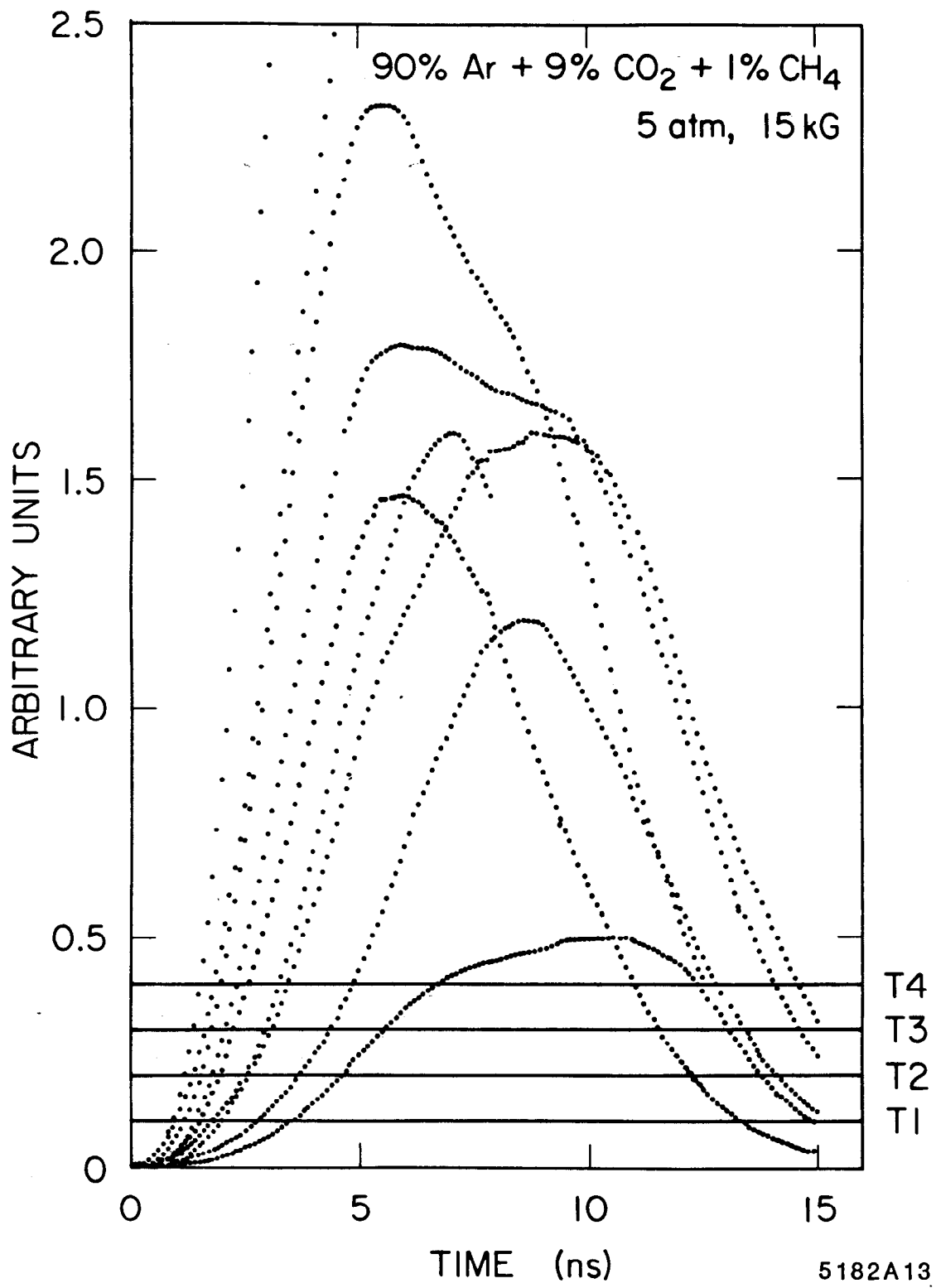
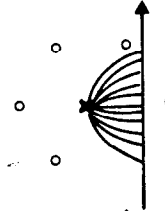
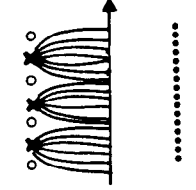


Fig. 8

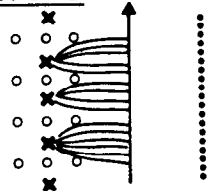
1) CYLINDRICAL



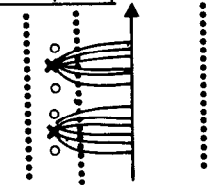
2) JET



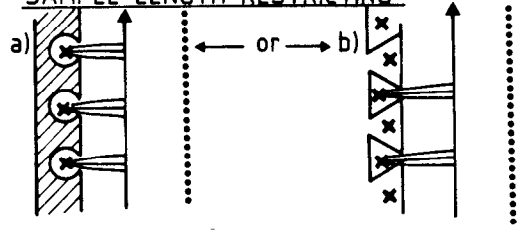
3) JET WITH FOCUSING



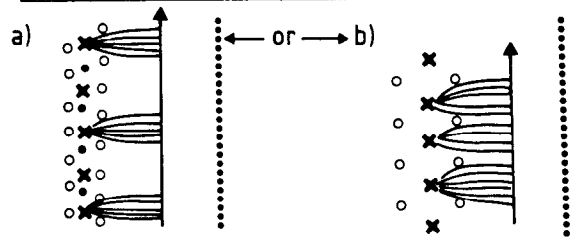
4) TIME EXPANSION (TEC)



5) SAMPLE LENGTH RESTRICTING



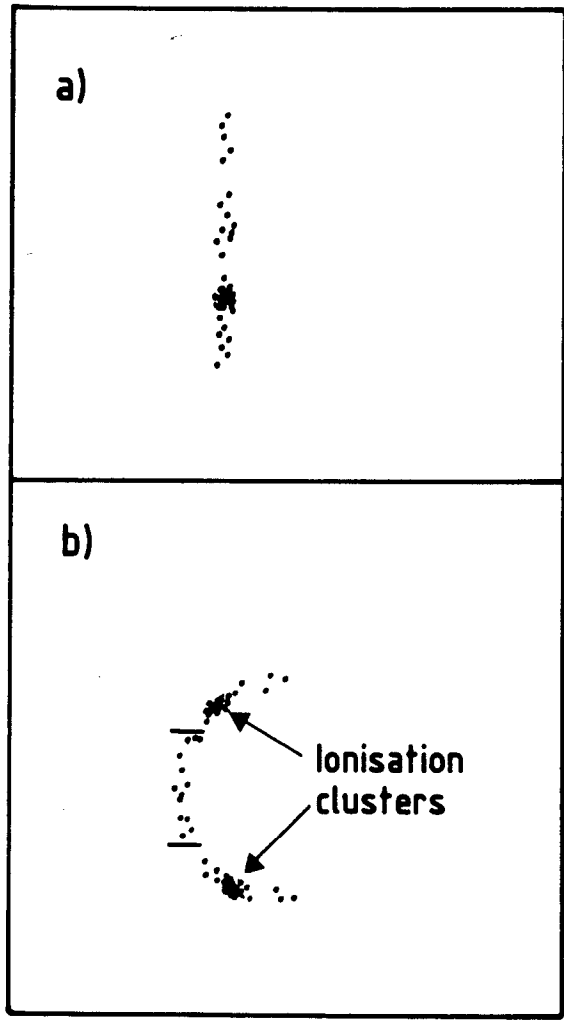
6) SPECIAL FOCUSING ARRANGEMENT



5182A14

Fig. 9

Position of drift electron along the sample



DRIFT TIME

5182A15

Fig. 10

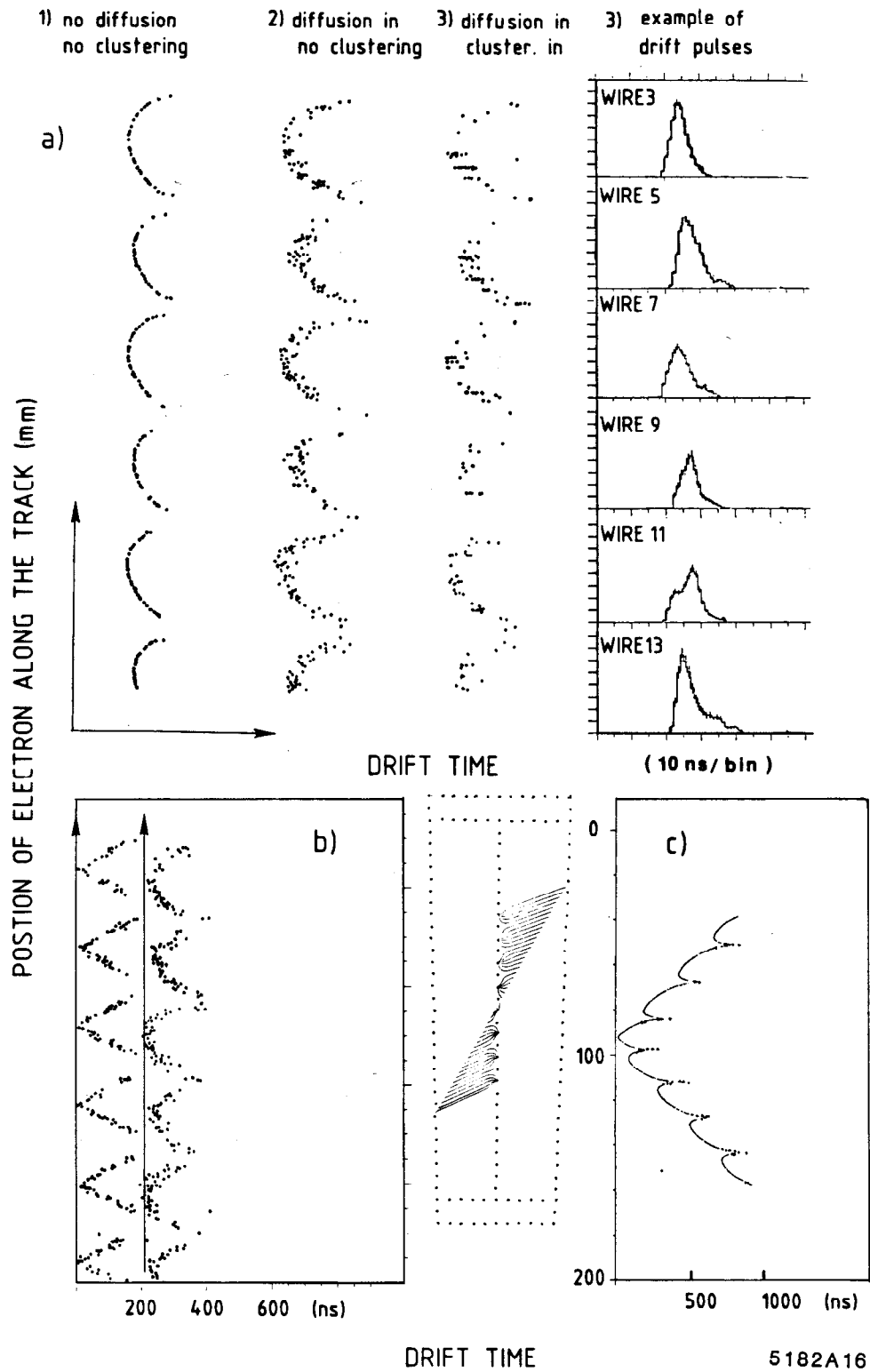


Fig. 11

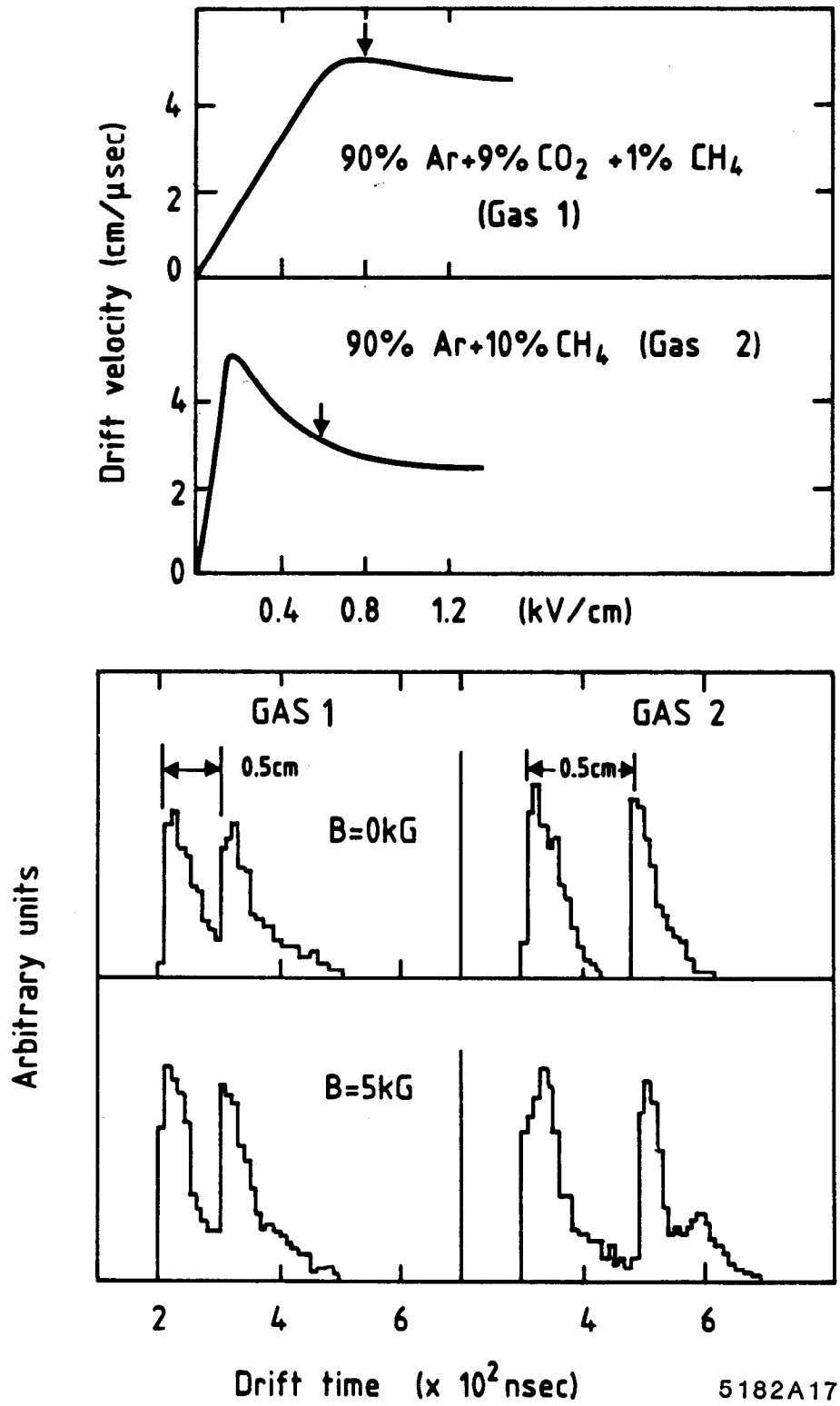
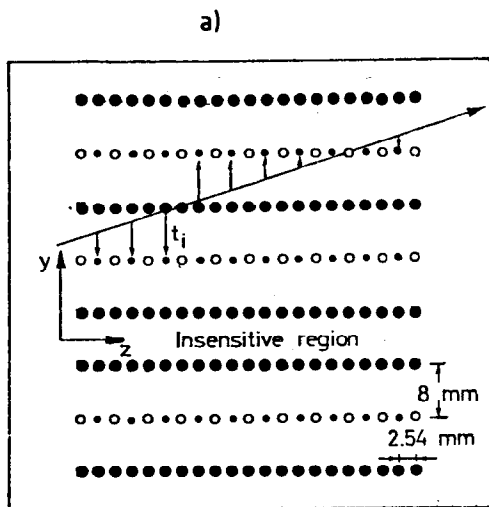
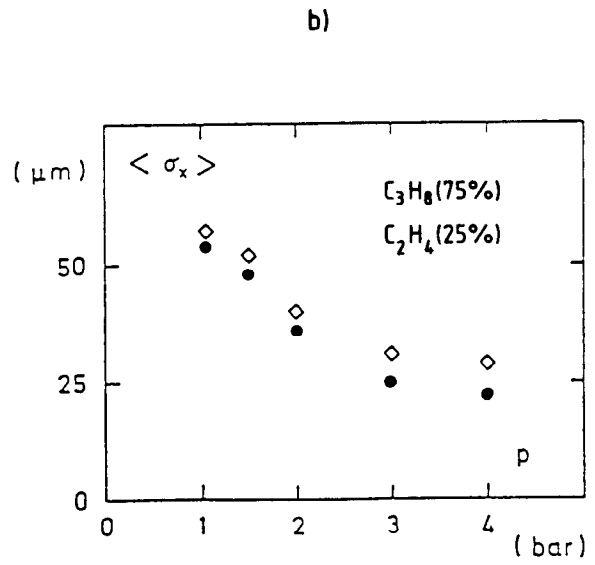


Fig. 12



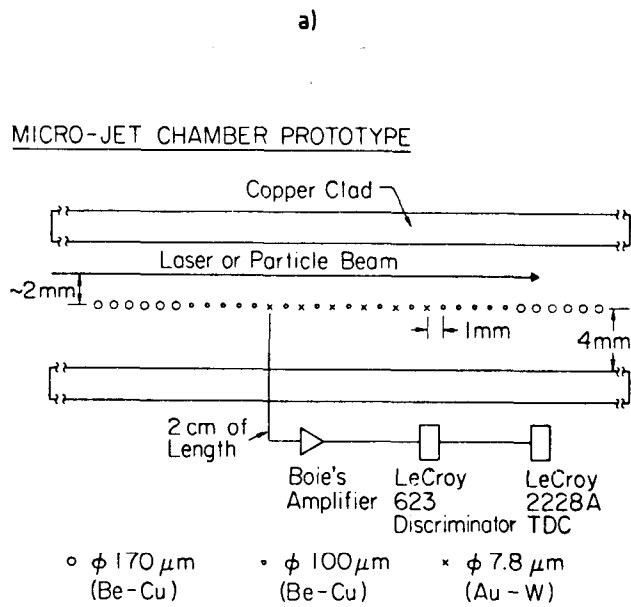
Diameter of cathode wires : ● 50 μ
 ■ 100 μ

Diameter of anode wires : • 10 μ
 ○ 20 μ



5182A18

Fig. 13



5182A19

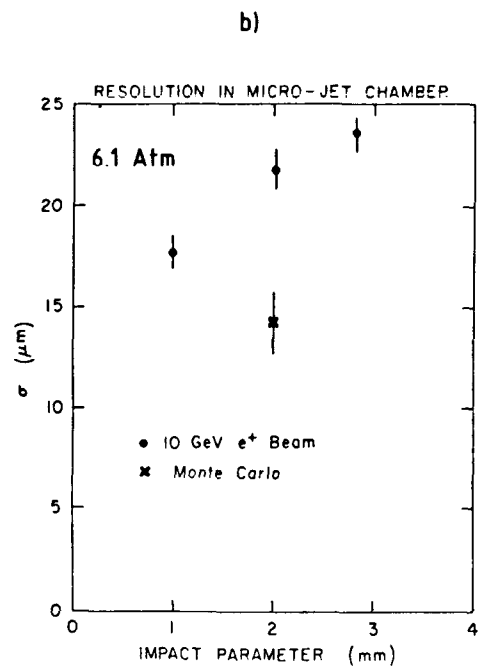
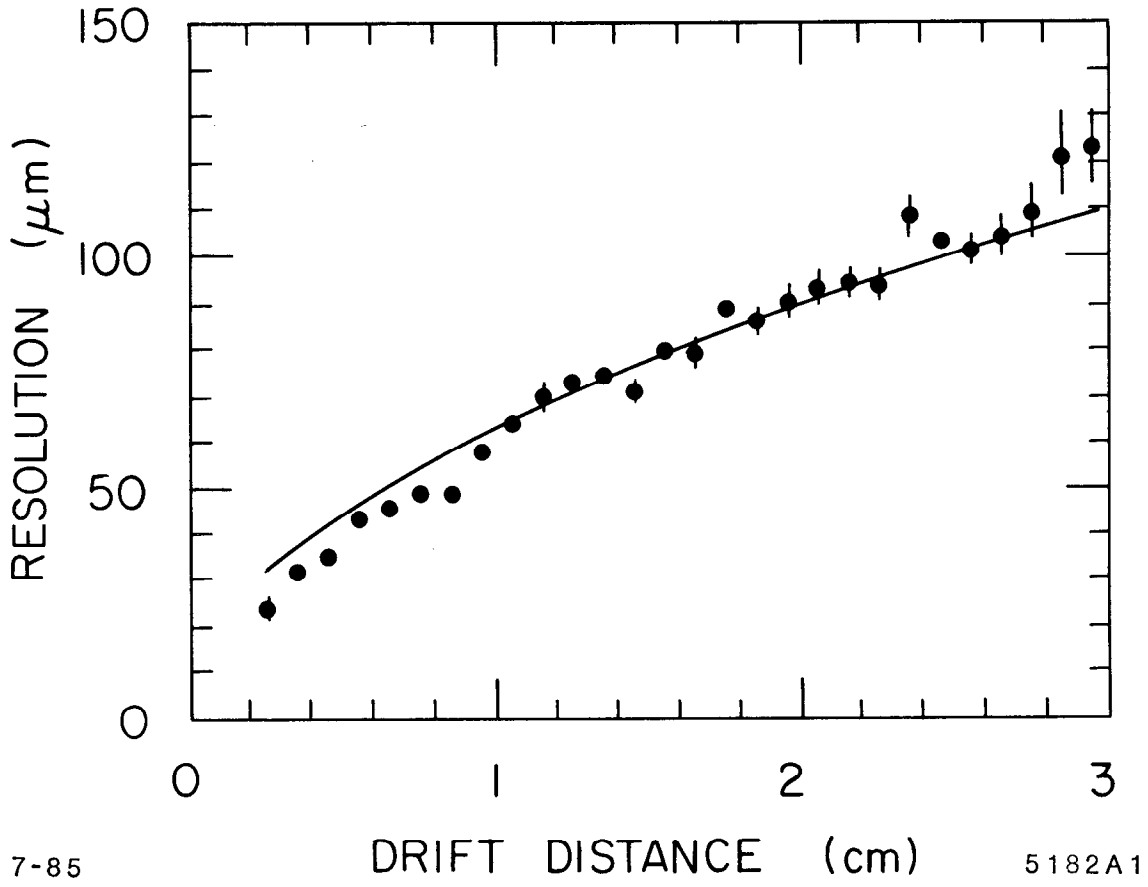


Fig. 14



7-85

DRIFT DISTANCE (cm)

5182A1

Fig. 15

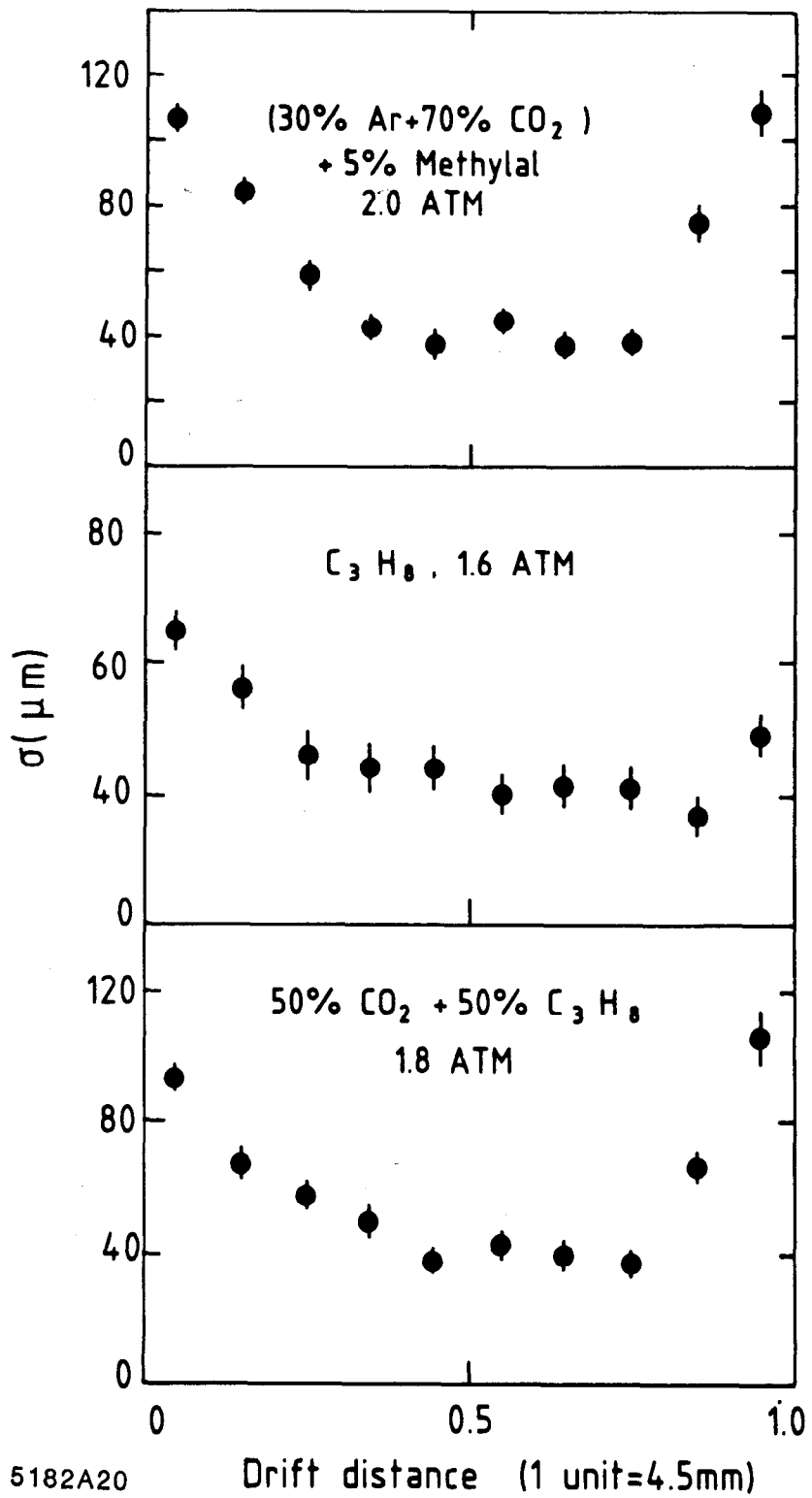
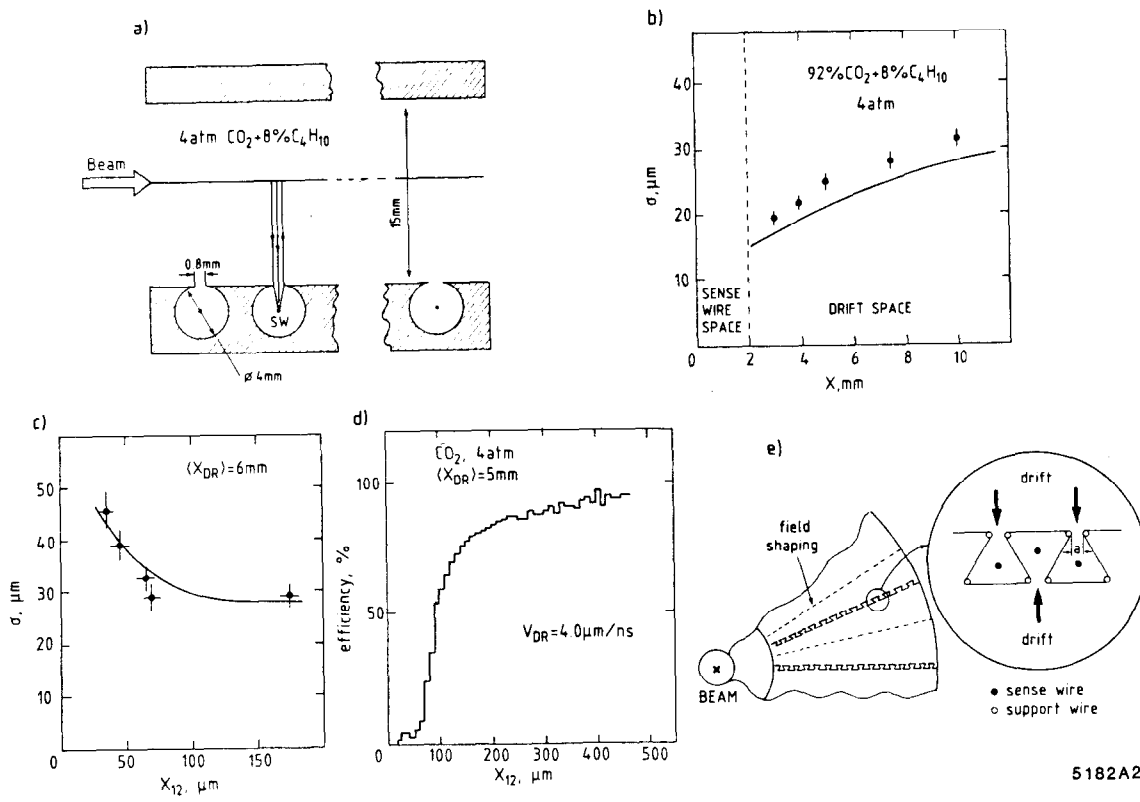


Fig. 16



5182A21

Fig. 17

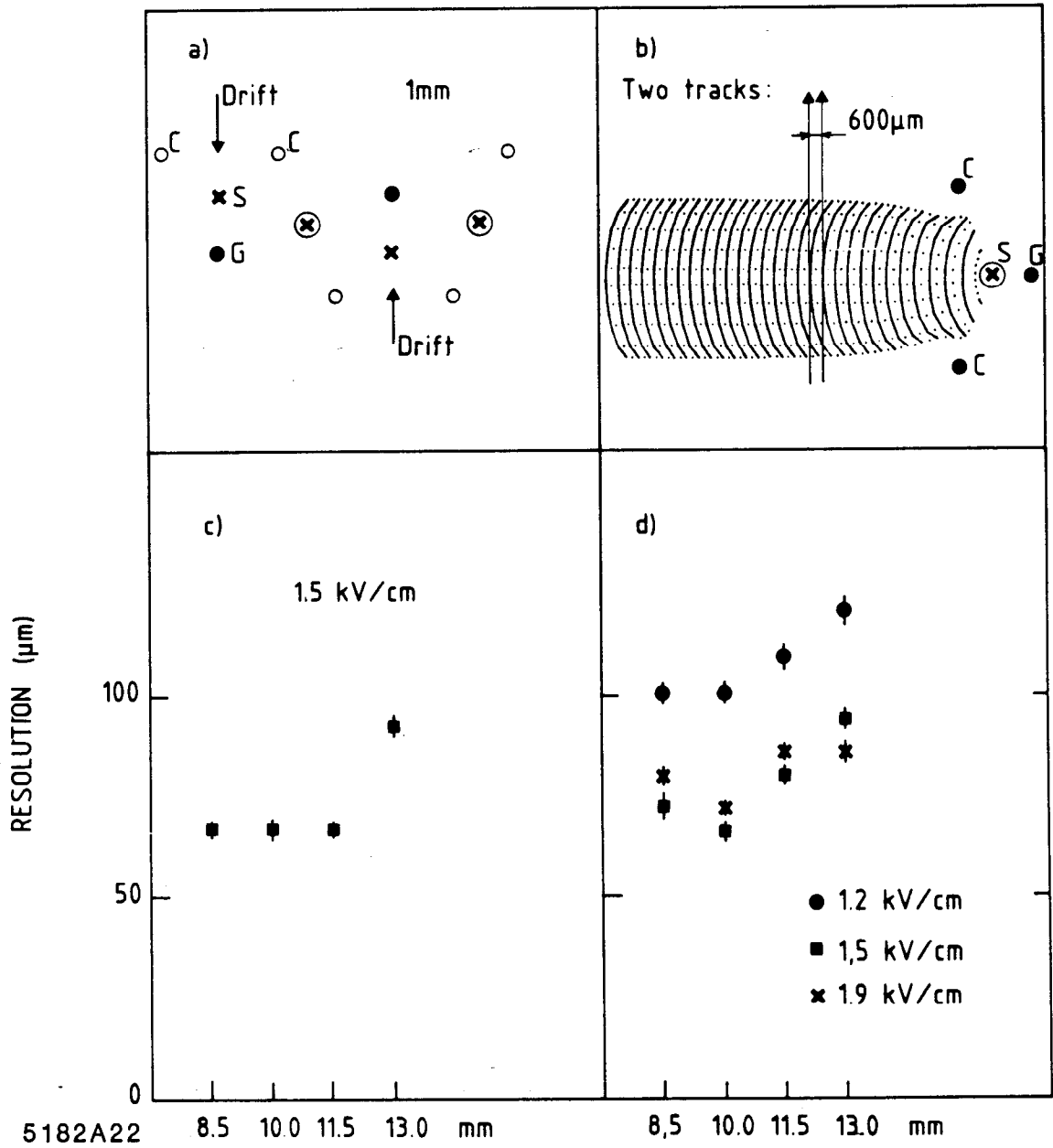


Fig. 18

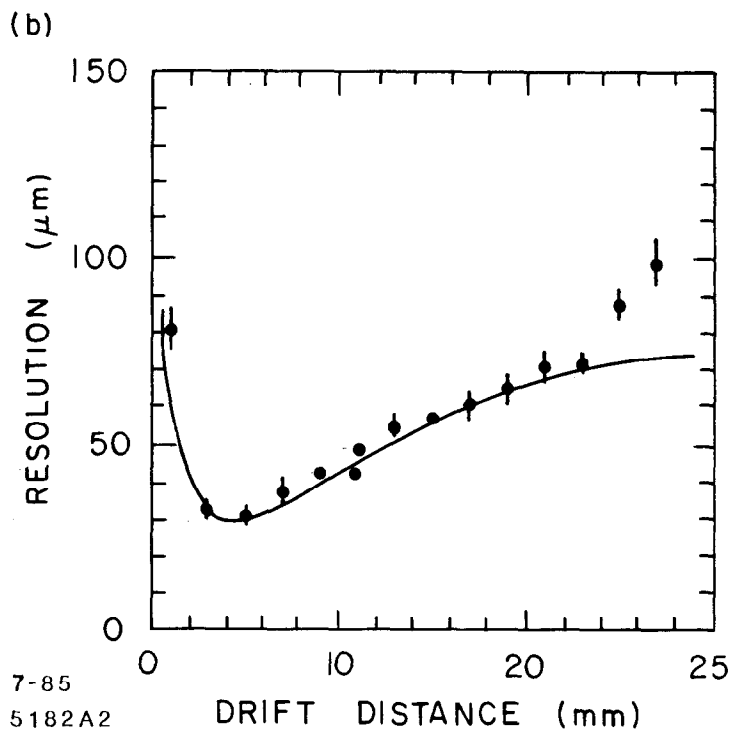
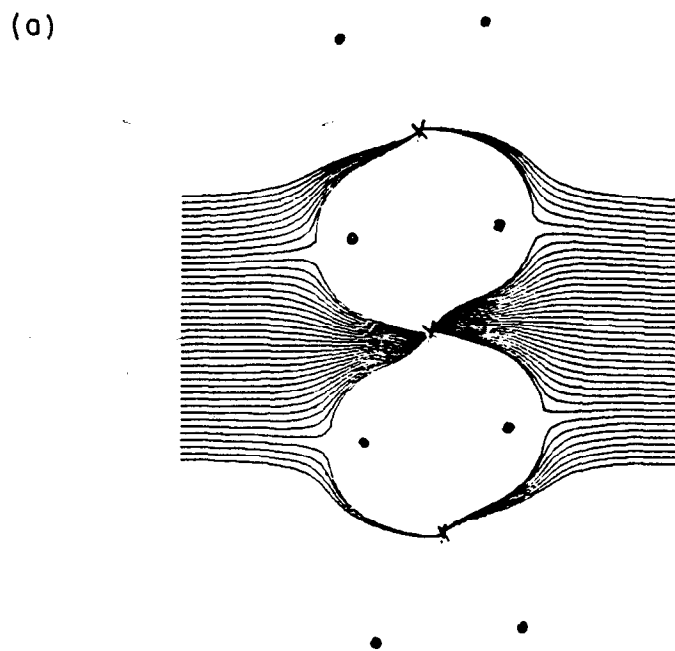
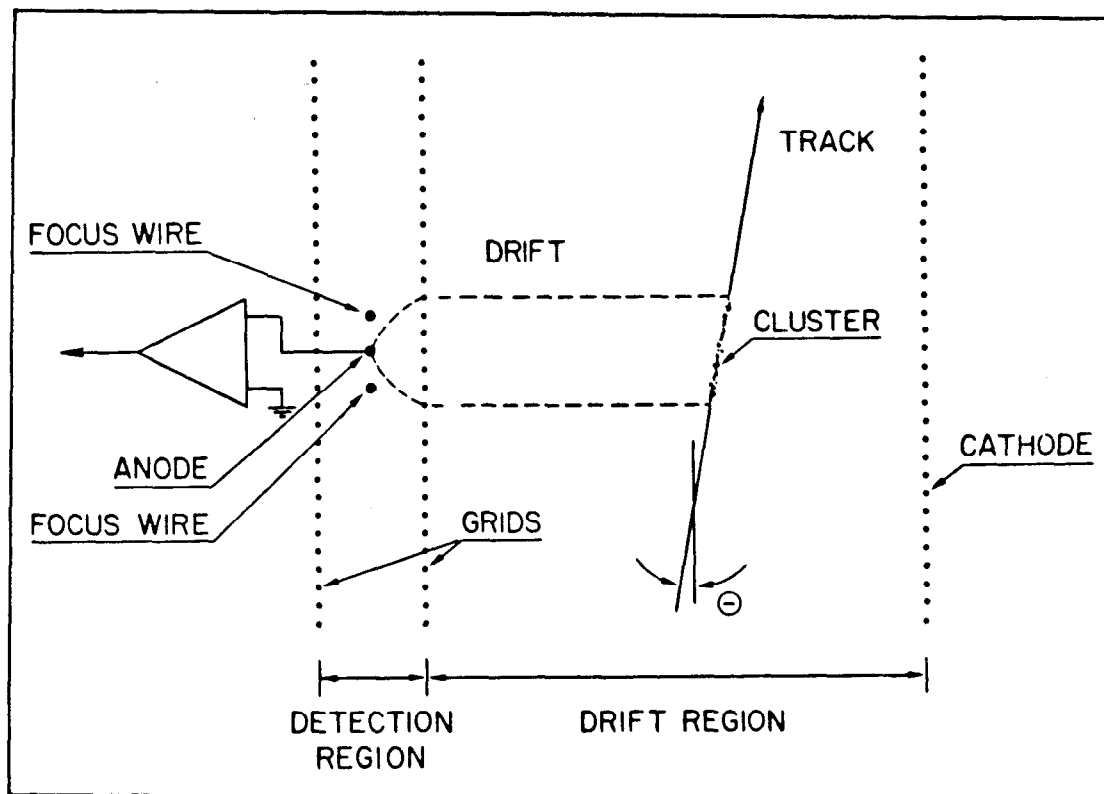


Fig. 19



5182A23

Fig. 20

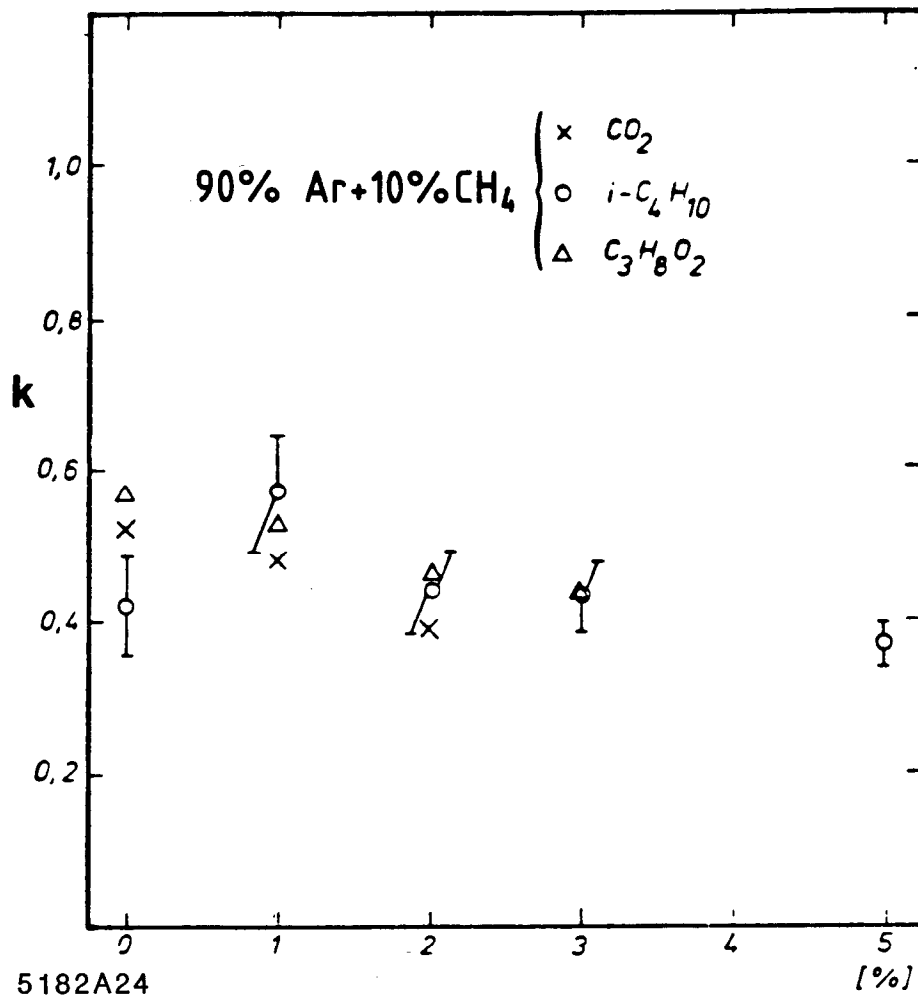


Fig. 21

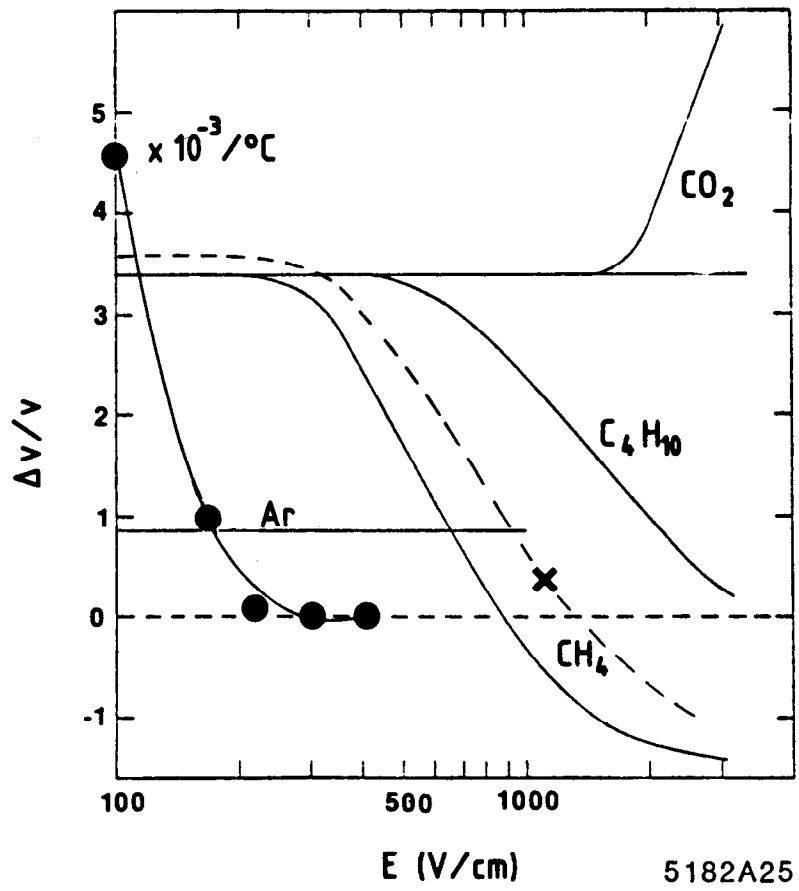
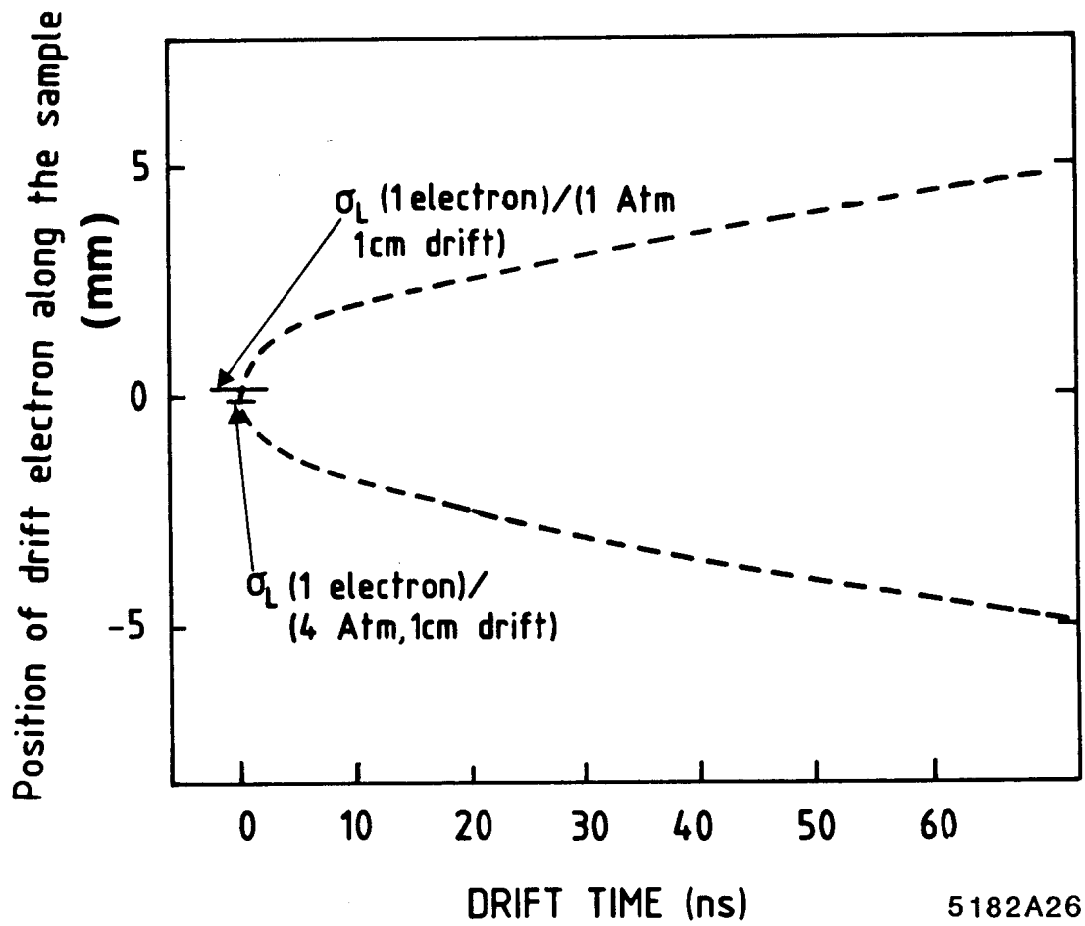


Fig. 22



5182A26

Fig. 23

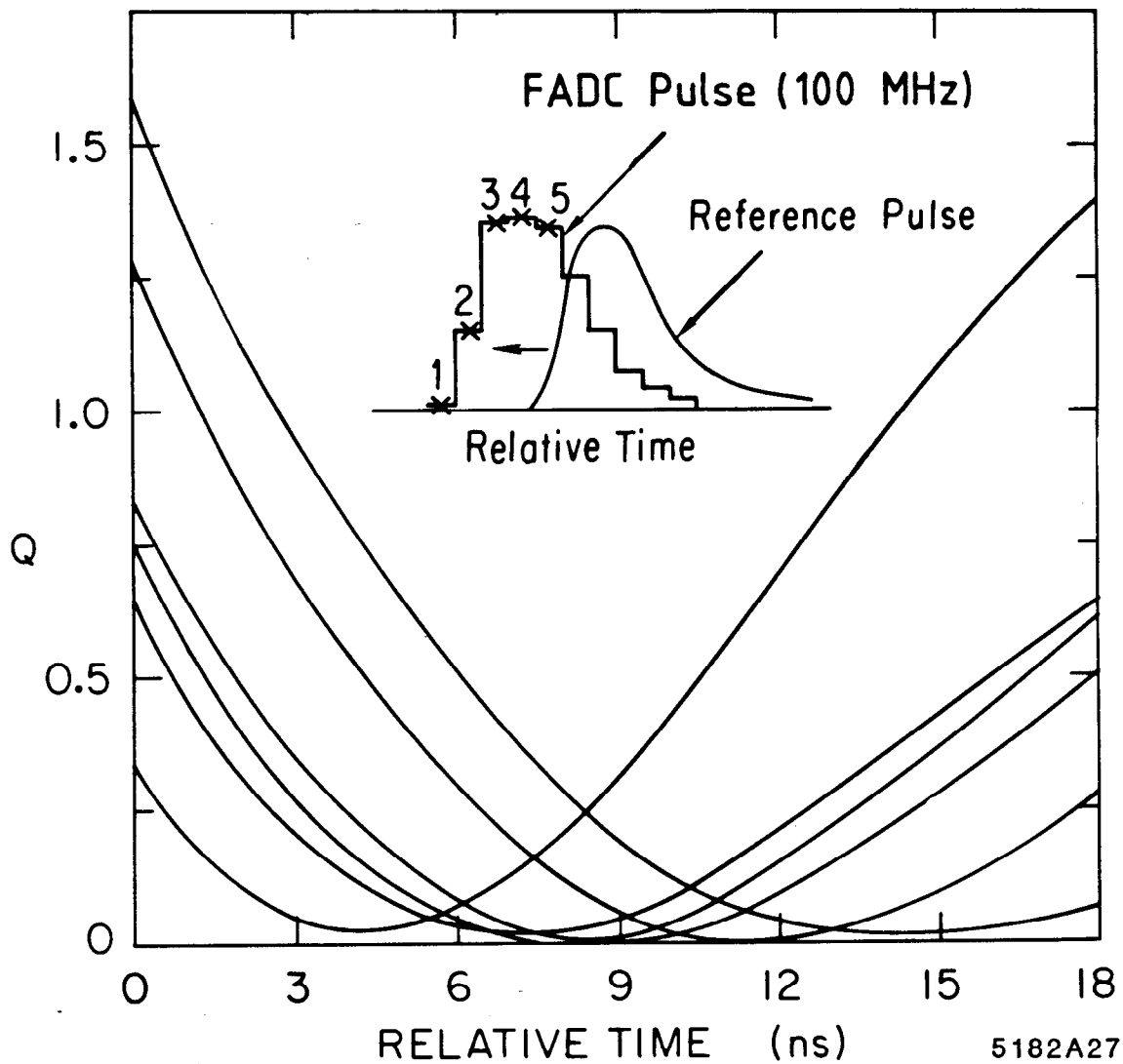


Fig. 24

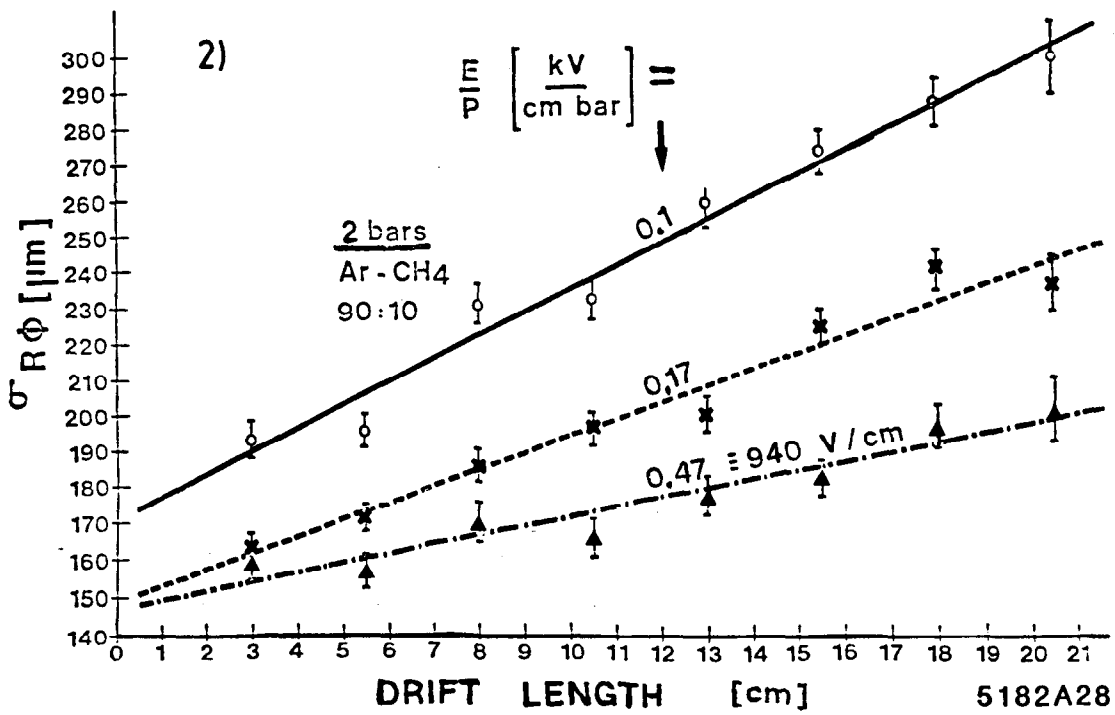
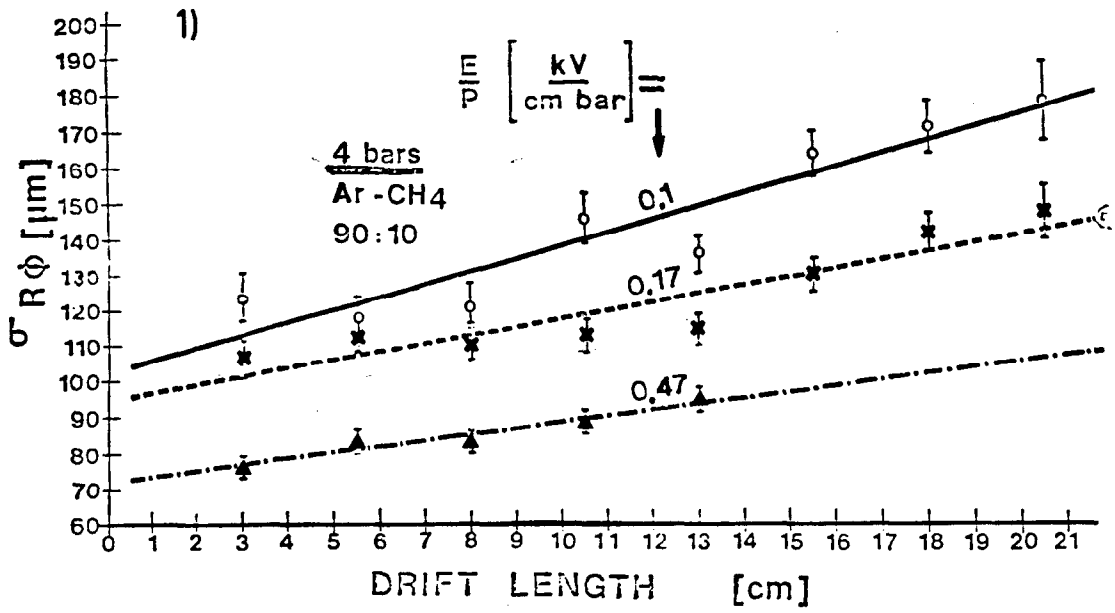


Fig. 25

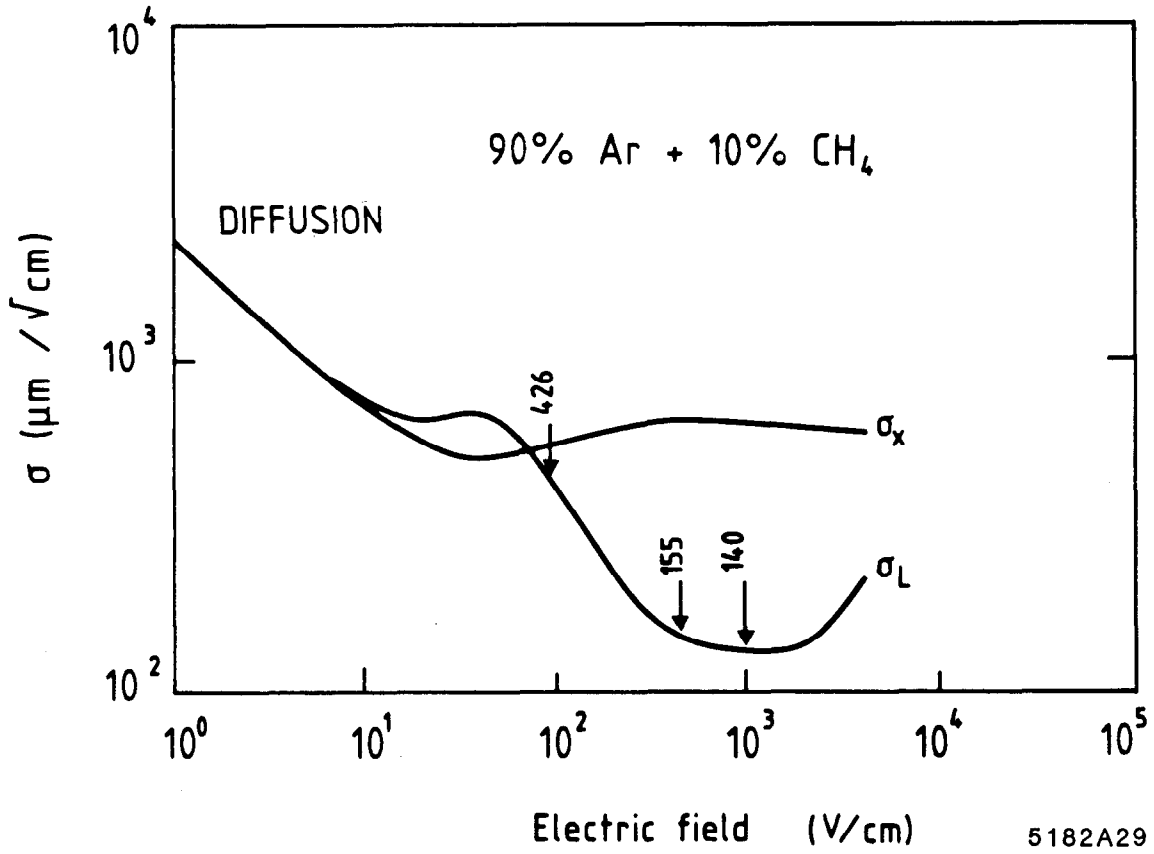


Fig. 26

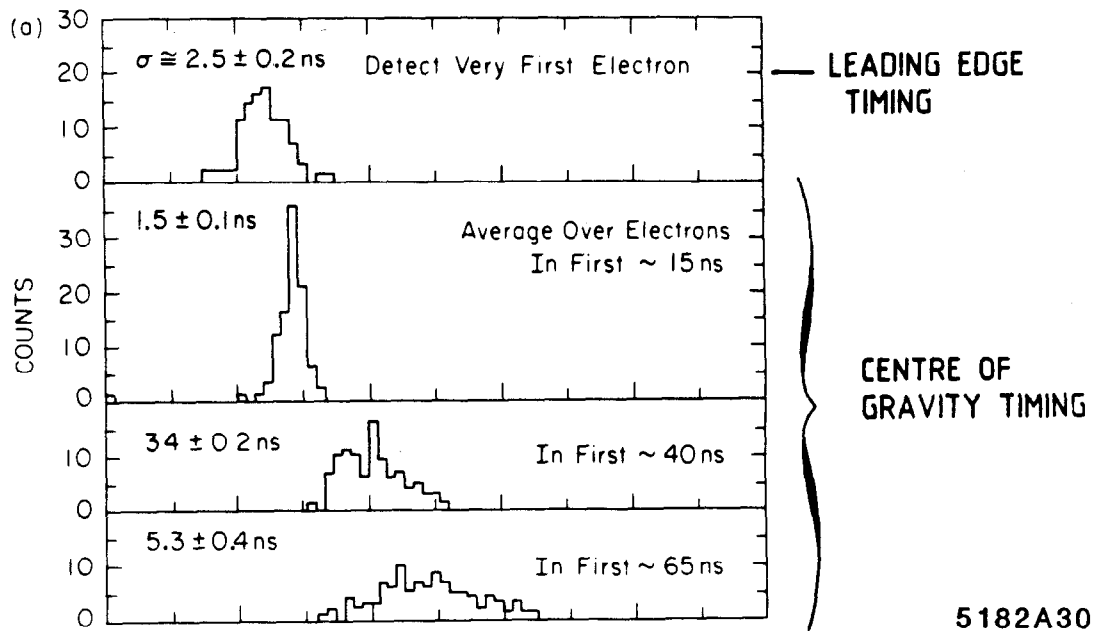


Fig. 27

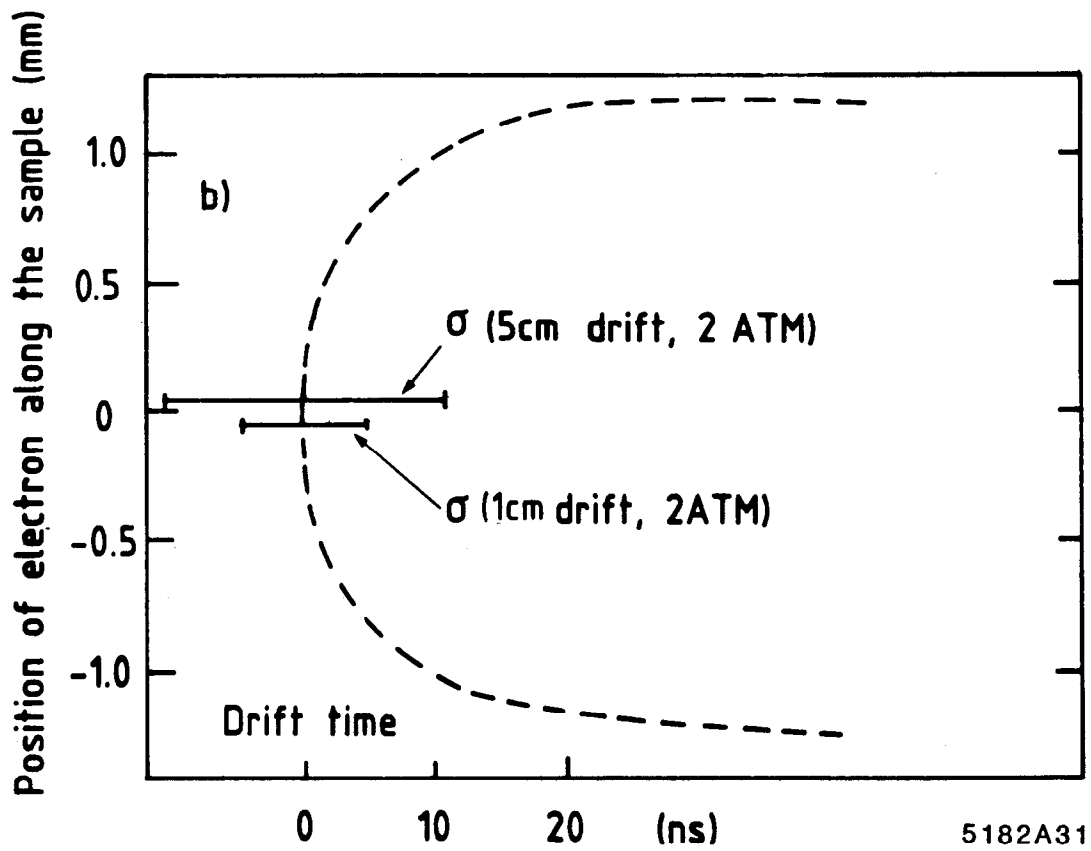
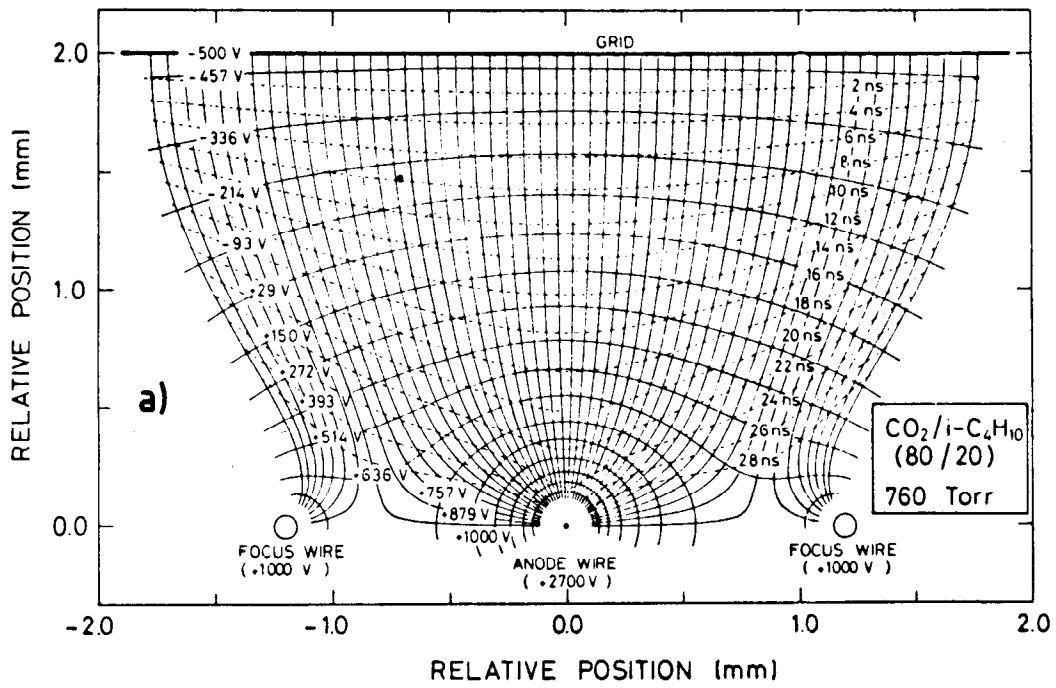


Fig. 28

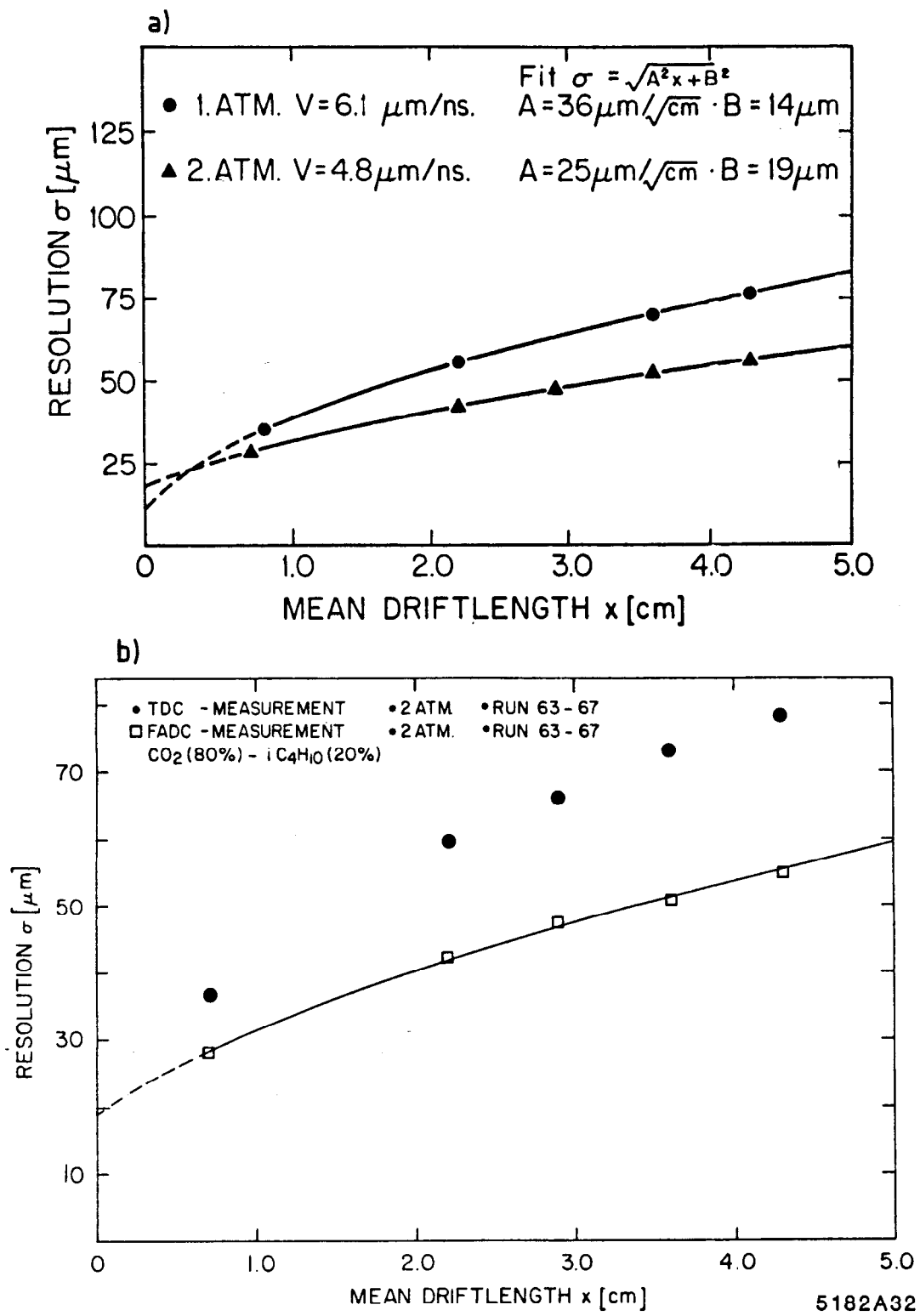


Fig. 29

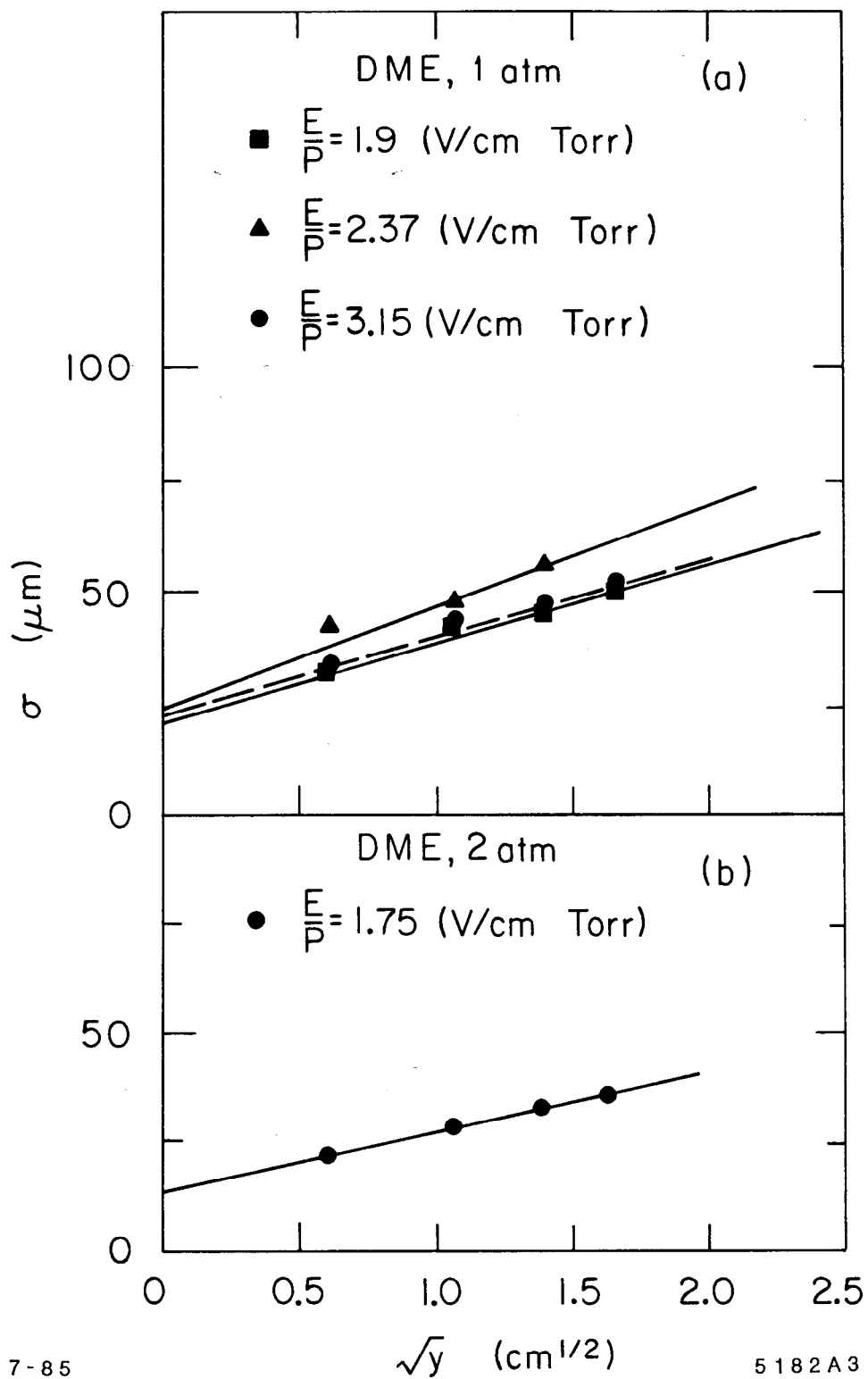


Fig. 30

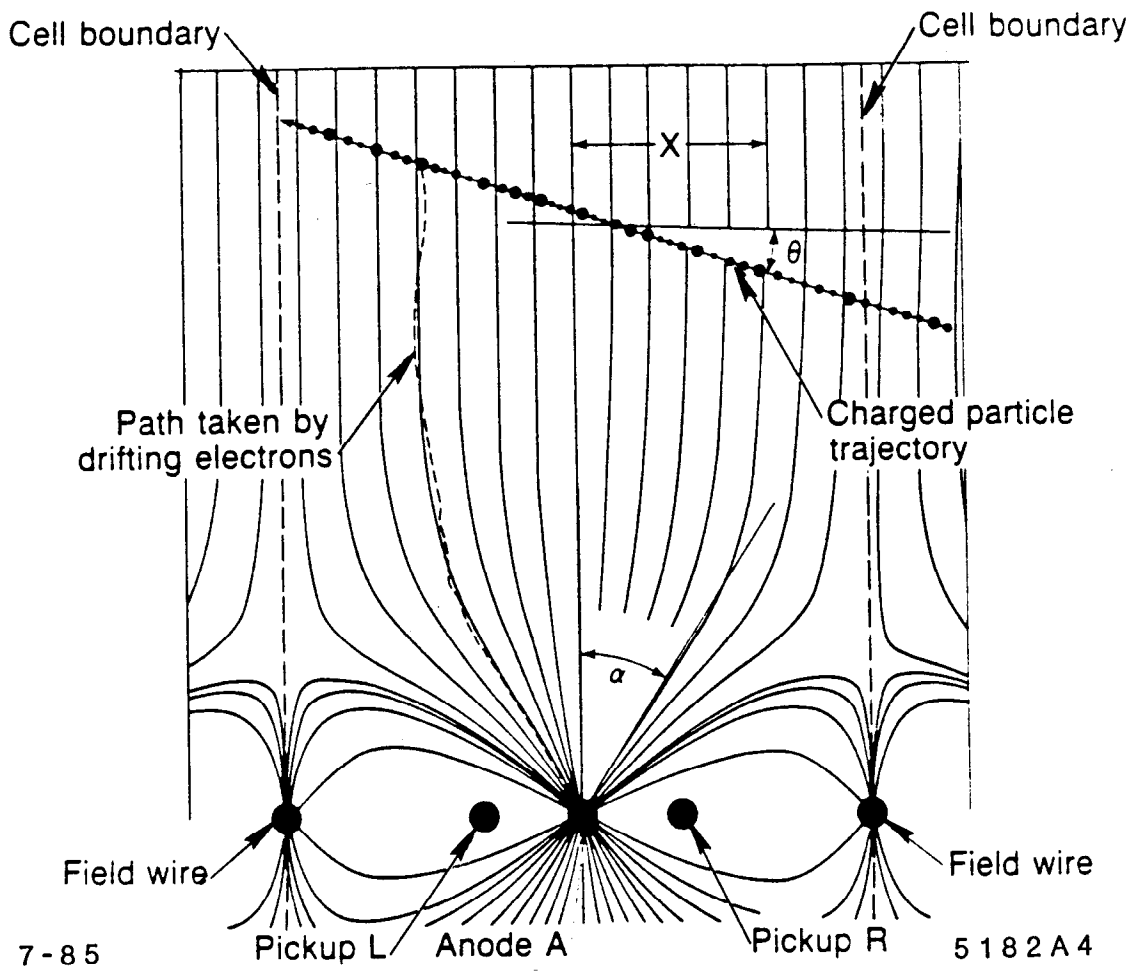
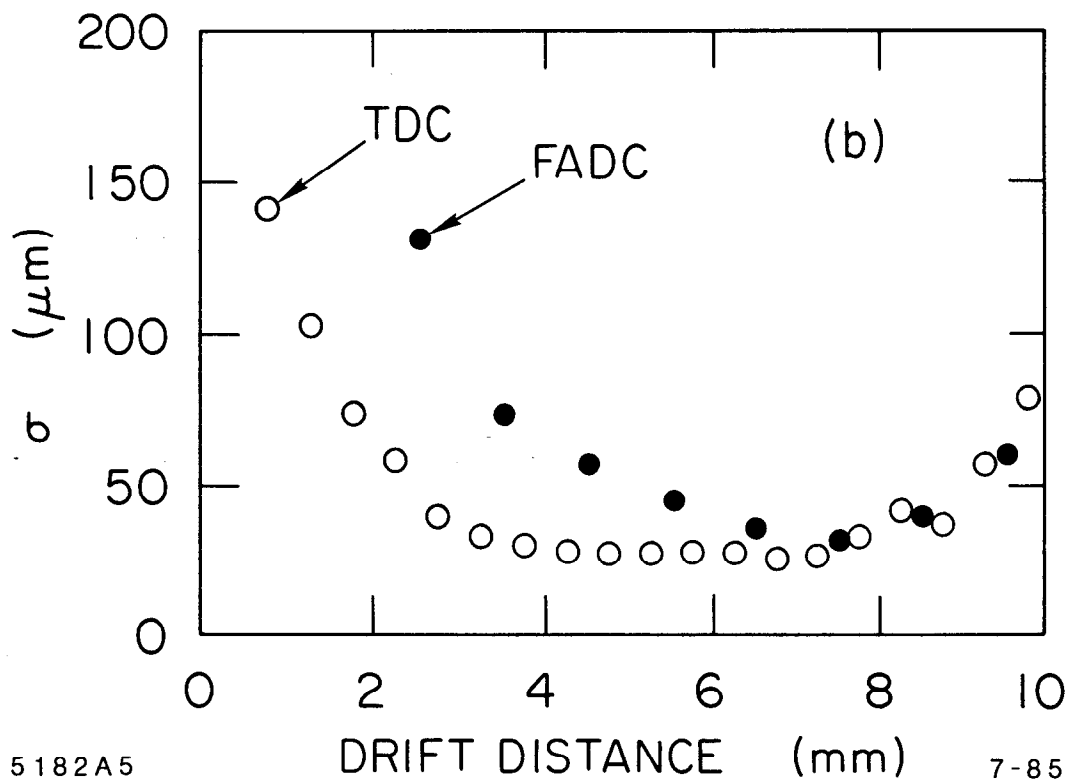
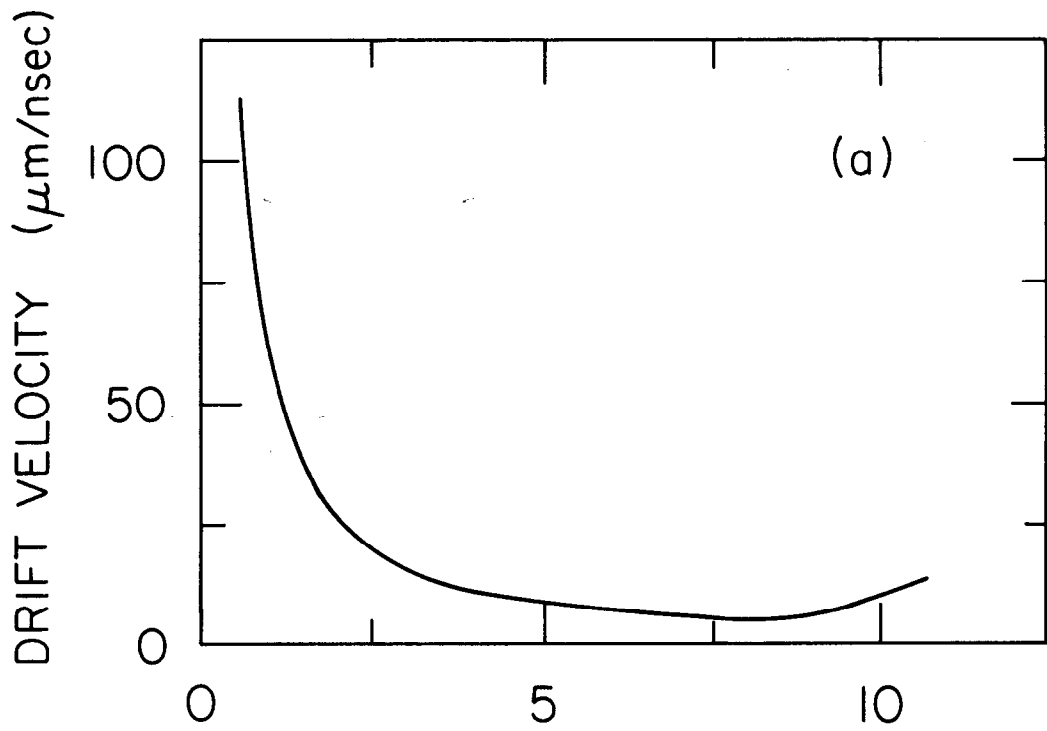


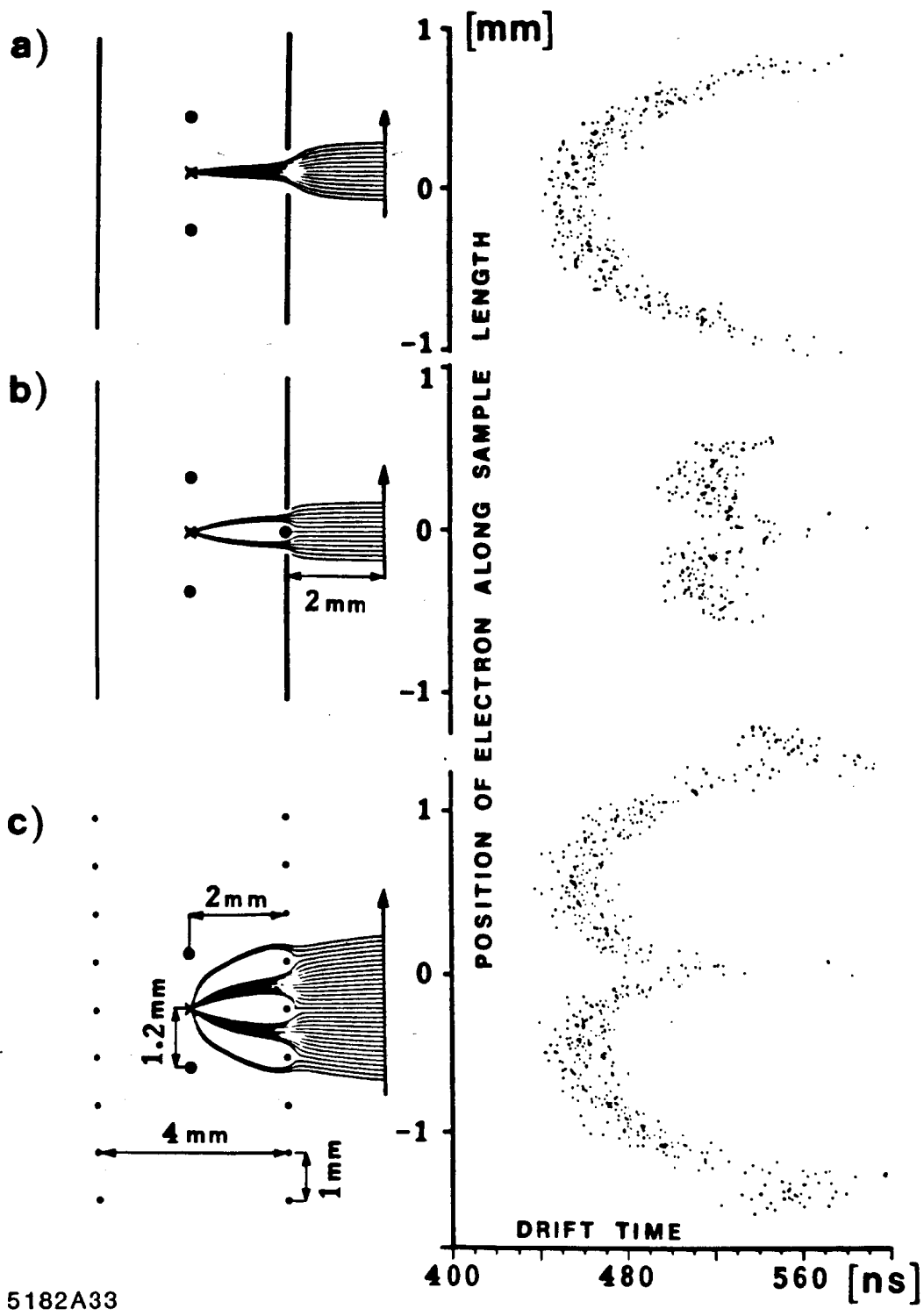
Fig. 31



5182A5

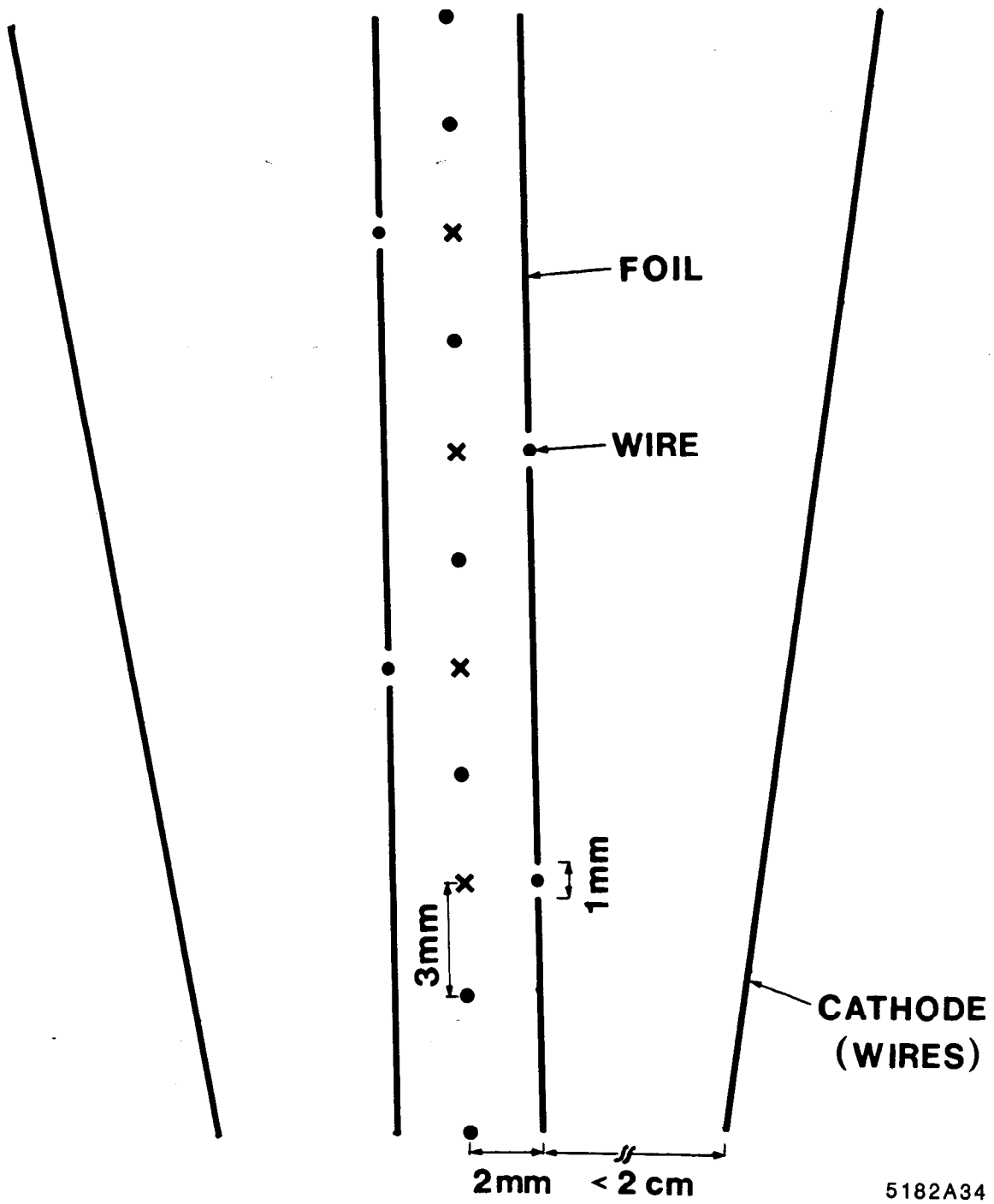
7-85

Fig. 32



5182A33

Fig. 33



5182A34

Fig. 34

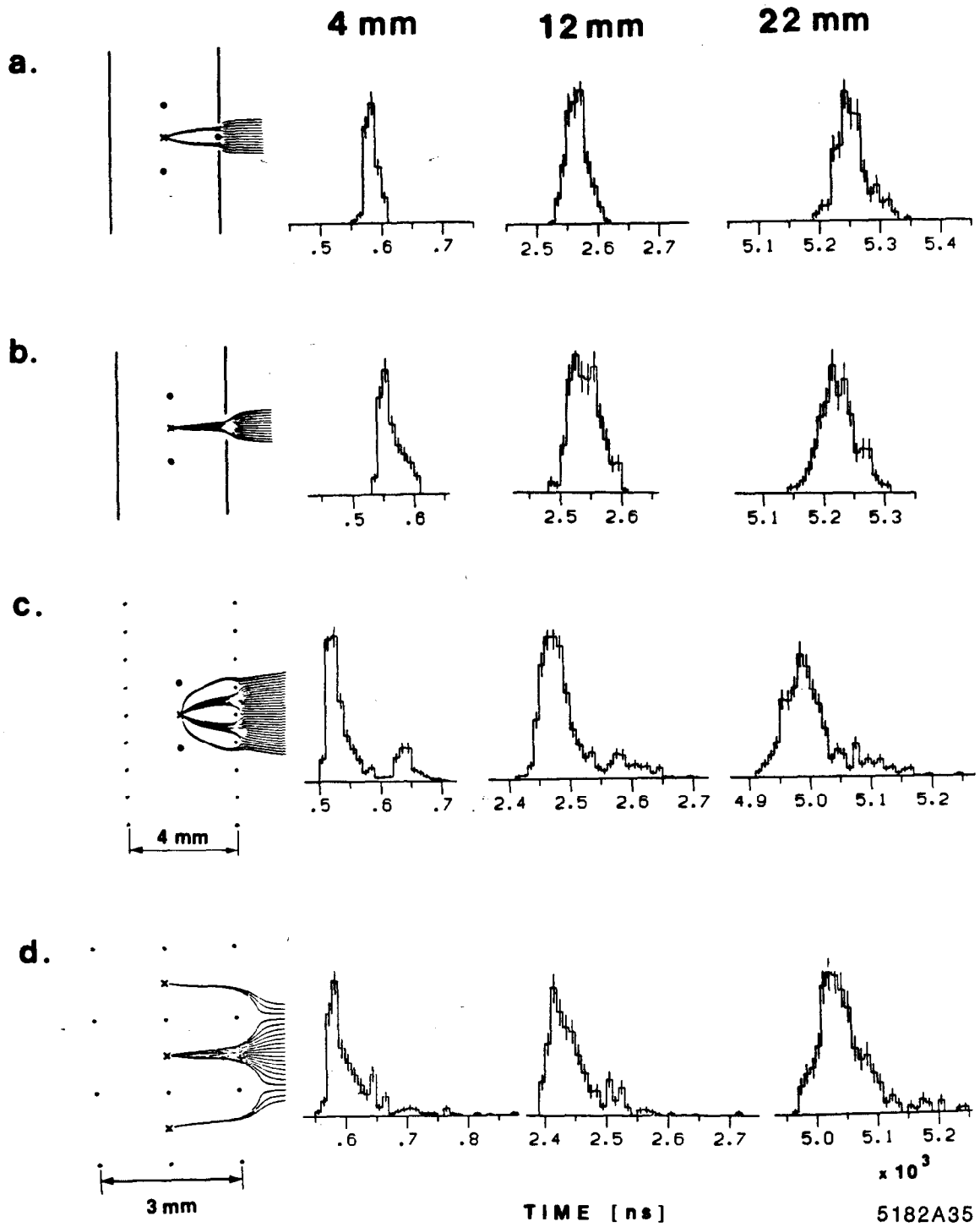


Fig. 35

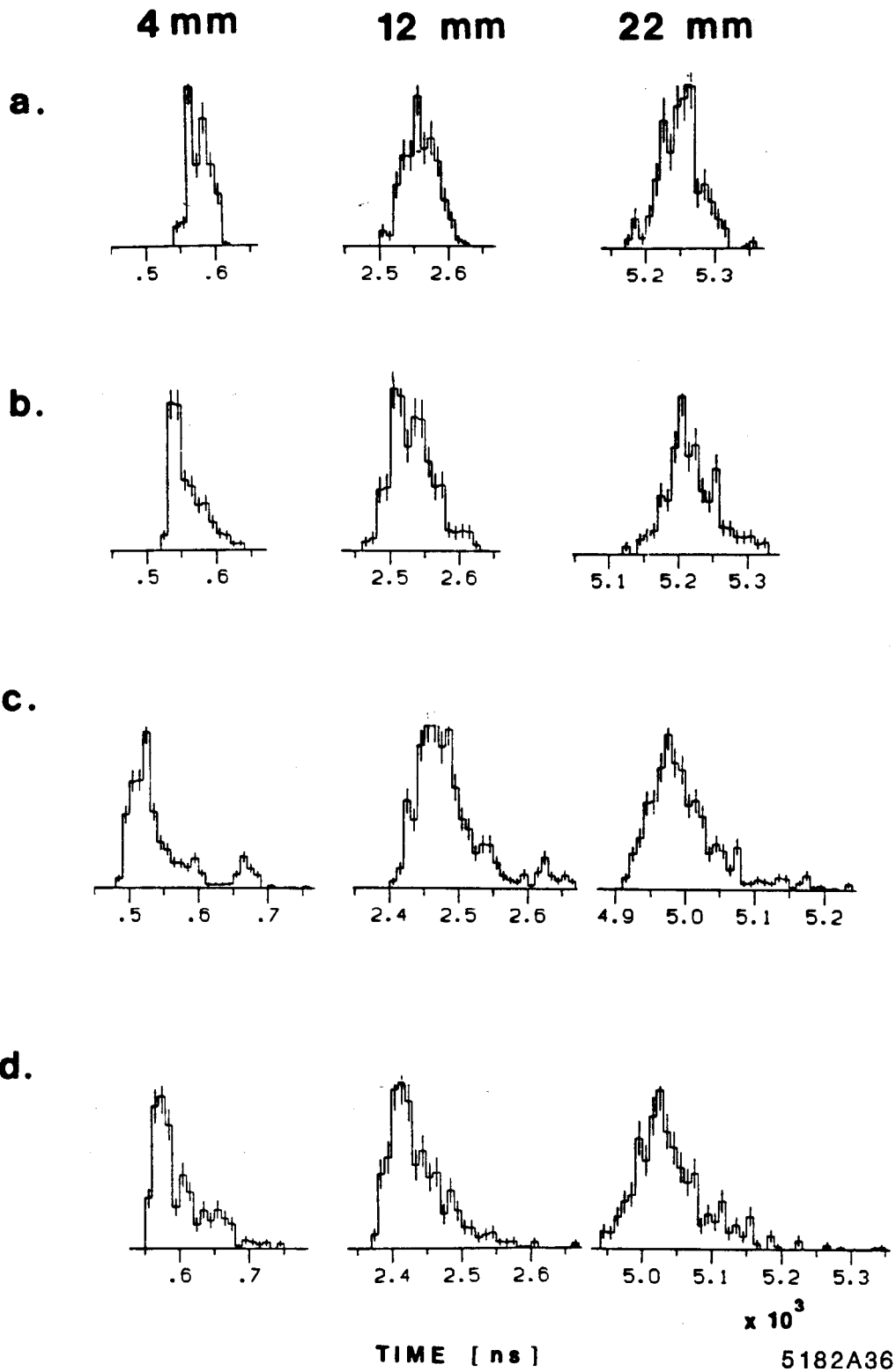


Fig. 36